IN-43
153103
P. 56

NASA
Technical
Memorandum

NASA TM - 108397

CALIBRATION, NAVIGATION, AND REGISTRATION OF MAMS DATA FOR FIFE

By G. J. Jedlovec and R. J. Atkinson

Space Science Laboratory

REPORT DOCUMENTATION PAGE

Form Approved
OMB No. 0704-0188

Public reporting burden for this collection of information is estimated to average 1 hour per response, including the time for reviewing instructions, searching existing data sources, gathering and maintaining the data needed, and completing and reviewing the collection of information. Send comments regarding this burden estimate or any other aspect of this collection of information, including suggestions for reducing this burden, to Washington Headquarters Services, Directorate for Information Operations and Reports, 1215 Jefferson Davis Highway, Suite 1204, Arlington, VA 22202-4302, and to the Office of Management and Budget, Paperwork Reduction Project (0704-0188), Washington, DC 20503.

1. AGENCY USE ONLY (Leave blank)	2. REPORT DATE	3. REPORT TYPE AND DATES COVERED
	February 1993	Technical Memorandum

4. TITLE AND SUBTITLE

Calibration, Navigation, and Registration of MAMS Data for FIFE

5. FUNDING NUMBERS

6. AUTHOR(S)

G. J. Jedlovec and R. J. Atkinson*

7. PERFORMING ORGANIZATION NAME(S) AND ADDRESS(ES)

George C. Marshall Space Flight Center
Marshall Space Flight Center, AL 35812

8. PERFORMING ORGANIZATION REPORT NUMBER

9. SPONSORING / MONITORING AGENCY NAME(S) AND ADDRESS(ES)

National Aeronautics and Space Administration
Washington, D.C. 20546

10. SPONSORING / MONITORING AGENCY REPORT NUMBER

NASA TM- 108397

11. SUPPLEMENTARY NOTES

Prepared by Space Science Laboratory, Science & Engineering Directorate.

*General Electric Company, Huntsville, Alabama

12a. DISTRIBUTION / AVAILABILITY STATEMENT

Unclassified--Unlimited

12b. DISTRIBUTION CODE

13. ABSTRACT *(Maximum 200 words)*

The International Satellite Land Surface Climatology Project (ISLSCP) was conducted to study the interaction of the atmosphere with the land surface and the research problems associated with the interpretation of satellite data over the Earth's land surface. The experimental objectives of the First ISLSCP Field Experiment (FIFE) were the simultaneous acquisition of satellite, atmospheric, and surface data and to use these data to understand the processes controlling energy/mass exchange at the surface. The experiment site is a 15 x 15 km area southeast of Manhattan, Kansas, intersected by Interstate 70 and Kansas highway 177. The Konza Prairie portion is 5 x 5 km and is a controlled experiment site consisting primarily of native tall grass prairie vegetation. The remainder of the site is grazing and farm land with trees along creek beds that are scattered over the area. Airborne multispectral imagery from the Multispectral Atmospheric Mapping Sensor (MAMS) was collected over this region on two days during Intensive Field Campaign -1 (IFC-1) to study the time and space variability of remotely-sensed geophysical parameters. These datasets consist of multiple overflights covering about a 60-min period during late morning on June 4, 1987, and shortly after dark on the following day. Image data from each overpass were calibrated and Earth located with respect to each other using aircraft inertial navigation system parameters and ground control points. These were the first MAMS flights made with 10-bit thermal data.

14. SUBJECT TERMS	15. NUMBER OF PAGES
MAMS, First ISLSCP Field Experiment, FIFE, Meteorology, Remote Sensing, Navigation, Calibration	56
	16. PRICE CODE: NTIS

17. SECURITY CLASSIFICATION OF REPORT	18. SECURITY CLASSIFICATION OF THIS PAGE	19. SECURITY CLASSIFICATION OF ABSTRACT	20. LIMITATION OF ABSTRACT
Unclassified	Unclassified	Unclassified	Unlimited

ACKNOWLEDGMENTS

Significant editorial and other contributions were made by Anthony Guillory/MSFC. His efforts are greatly appreciated. Portions of this work were performed under the Physical Climate and Hydrologic Systems research program at NASA Headquarters. The support of the MAMS flights for FIFE by Dr. James Dodge is greatly appreciated. The collection of the MAMS data was also possible because of the dedicated efforts of various NASA Ames Research Center personnel, including the instrument technicians, U2 flight crew and pilots.

TABLE OF CONTENTS

	Page
INTRODUCTION	1
Applications of the MAMS	1
Purpose of MAMS Flights During FIFE	1
BACKGROUND	3
Instrument Description	3
MAMS FIFE Data	7
CALIBRATION	12
Visible Channels	12
Infrared Channels	13
NAVIGATION	16
Data Sources	16
The Algorithm	17
Navigation Correction Using Landmarks	17
Navigation Correction During Remapping	20
Universal Transverse Mercator (UTM) Grid System	28
Projection Formulas	30
FIS DATASET	34
Data Quality	34
JOURNAL OF GEOPHYSICAL RESEARCH (JGR) DATASET	37
SUMMARY	38
REFERENCES	39
APPENDIX	41

LIST OF ILLUSTRATIONS

Figure	Title	Page
1	MAMS scan geometry	4
2	MAMS flight tracks over the FIFE study region	9
3	Aircraft roll data from INS and MAMS data streams	18
4	Landmark-determined and INS headings	21
5	Landmark-determined headings and corrected regression fit of headings	23
6	Regression fit of pitch with spurious readings ignored	26
7	Displacements after remapping FIFE passes 1 and 2 into UTM coordinates	27
8	Transverse Mercator projection geometry	29
A1	MAMS raw imagery	42

LIST OF TABLES

Table	Title	Page
1	Selected Multispectral Scanner Characteristics	5
2	Comparison of Satellite Thermal Channel Characteristics with that of MAMS	6
3	Standard MAMS Instrument Configuration	8
4	Channel Sensitivities and Sample Noise Estimates for MAMS Channels for FIFE on June 4, 1987	11
5	Landmark RMS Errors	25
6	FIS Data Coverage Region	35
7	MAMS FIS Data	36

TECHNICAL MEMORANDUM

CALIBRATION, NAVIGATION, AND REGISTRATION OF MAMS DATA FOR FIFE

INTRODUCTION

NASA developed several aircraft sensors in the mid 1980's to verify data from new satellite sensors and to collect unique datasets that would serve to justify future space-based instruments on low-Earth and geostationary observation platforms. In 1985, the Multispectral Atmospheric Mapping Sensor (MAMS) was developed and flown to verify small-scale water vapor features observed in Visible Infrared Spin Scan Radiometer (VISSR) Atmospheric Sounder (VAS) imagery on the Geosynchronous Operational Environmental Satellites (GOES). This aircraft sensor provided a unique opportunity to independently verify single pixel variations observed in the VAS channels (Menzel et al., 1986). This verification continued for several years providing useful correlative measurements (Jedlovec et al., 1986b; Moeller et al., 1990).

Applications of the MAMS

The MAMS 6.5 micrometer channel has been used to map variations in upper tropospheric water vapor associated with a variety of atmospheric disturbances (Menzel et al., 1986; Jedlovec et al., 1986b). The split window channels at 11 and 12 μm allow surface temperature estimations and the determination of the total integrated water content in a column of the atmosphere as discussed by Jedlovec (1987, 1990). The MAMS has also been used to study geomorphology along the Gulf of Mexico coast. Reflectances in the visible and near infrared channels of MAMS have been used to estimate suspended sediment concentrations, their source regions, and spatial distribution. Data from a series of flights before and after passage of weather systems have enhanced the understanding of the role that these systems play in producing geomorphic changes (Moeller et al., 1989). A time sequence of multispectral imagery along the coast of California was collected in October of 1989 to investigate the feasibility of determining ocean motions by tracking features in the water. MAMS data have been collected over Mt. Mitchell, North Carolina to detect and monitor the effects of pollution on forest decline in the region.

Purpose of MAMS Flights During FIFE

In 1987, a series of flights was initiated to collect several unique datasets which capture the spatial and temporal variability of atmospheric and surface geophysical parameters important to small-scale hydrologic and energy processes of the surface and lower atmosphere. A secondary goal was to study the problems with remote

sensing of geophysical parameters from geostationary orbit, particularly with respect to the changing satellite-Sun viewing geometries. These flights included several over the FIFE region. The specific goals of the FIFE flights were to investigate the thermal variability of the surface over a highly instrumented ground-truth site, its relation to surface features, land use, and soil moisture, and to study the effect of different Sun-sensor viewing geometries on the visible and reflected infrared measurements. The above goals also addressed several of the FIFE scientific objectives, particularly those dealing with the correction and calibration of remotely-sensed data, and the measurement of reflected and emitted radiances for biological process studies (Sellers and Hall, 1987).

The data collected with MAMS over the FIFE region provide unique visible and infrared measurements of the atmosphere and underlying surface at time and space scales currently not available from satellites. This document describes the MAMS dataset for FIFE, the data quality, spatial resolution, data coverage, and the calibration and navigation procedures employed. A comprehensive analysis of the MAMS thermal data has been performed and used to study the relationship between surface thermal parameters and surface features as represented by their NDVI values. A review of MAMS-derived geophysical parameters for FIFE is presented in Jedlovec and Atkinson (1992).

BACKGROUND

The aircraft remote sensing data used in this investigation are from the airborne Multispectral Atmospheric Mapping Sensor (MAMS) (Jedlovec et al., 1986a, 1989). MAMS is a multispectral scanner that measures reflected radiation from the Earth's surface and clouds in eight visible and near infrared bands, and thermal emission from the earth's surface, clouds, and atmospheric constituents (primarily water vapor) in three of four available infrared bands.

Instrument Description

The MAMS scan geometry is shown in Figure 1. The instrument was flown on a NASA U2 high-altitude aircraft during FIFE at a nominal altitude of 20 km, and provided a horizontal ground resolution for each field-of-view of about 100 m at nadir. From this altitude, the width of the entire cross path field-of-view scanned by the sensor was roughly 37 km and provided detailed resolution of atmospheric and surface features across the swath width and along the aircraft flight track.

The MAMS design was based on that of other instruments developed by Daedalus Enterprises, Inc. for visible and infrared mapping. It shares the same scan head, digitizer, tape system, and supporting electronics as other Daedalus airborne scanners for the NASA high altitude aircraft. The difference lies in the spectrometer channels, particularly in the infrared region (Jedlovec et al., 1986a). The prism used to disperse the incident energy into the visible and near infrared channels is identical to that of the airborne Thematic Mapper Simulator (TMS). The use of the 5.0 mRa aperture in the standard MAMS configuration, however, changes the spectral characteristics of the near infrared channels slightly as shown in Table 1. This difference does not significantly affect the use of the MAMS channels for surface applications. Four of the MAMS visible and near-infrared channels are similar to the first four channels of the Thematic Mapper (TM) on Landsat. Therefore, these channels can be used in similar applications.

MAMS is somewhat unique compared to other airborne scanners, since it provides some additional thermal infrared channels which have similarity to other satellite sensors. The infrared channels from MAMS have commonality with those from the Advanced High Resolution Radiometer (AVHRR) and VAS sensors on existing weather satellites. The single thermal channel of the Landsat Thematic Mapper covers a broader spectral range than the MAMS. Spectral response characteristics for these common channels are presented in Table 2. The 11 μm channels of MAMS and VAS are very similar while that of the AVHRR is narrower and shifted toward

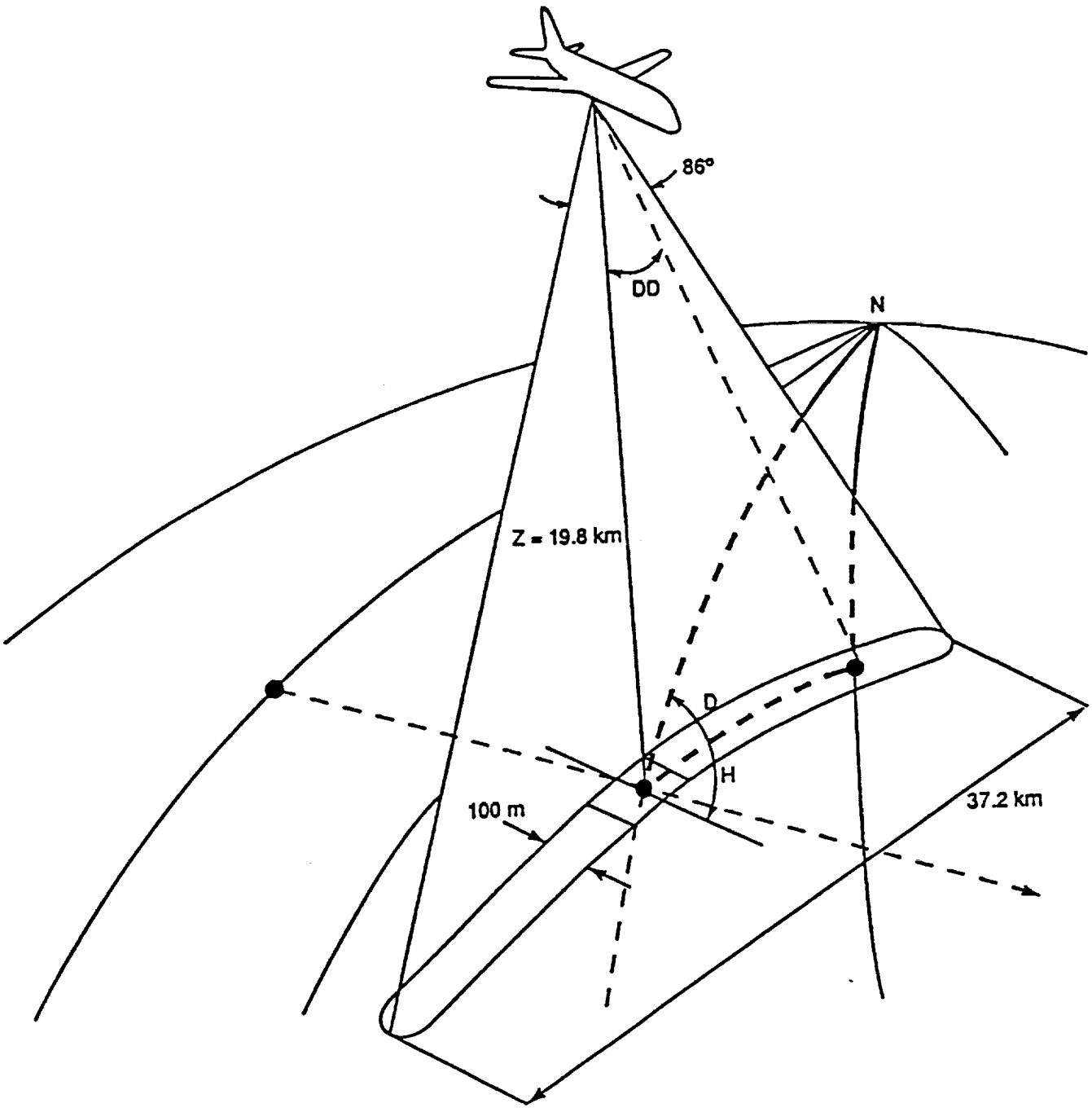


Figure 1. MAMS scan geometry.

Table 1. Selected multispectral scanner channel characteristics

	Visible Channels Bandwidth (@50% repsonse)		
Channel	SPOT	Landsat TM	MAMS @ 5.0 mRa
1		0.45-0.52	0.42-0.45[a]
2		0.52-0.60	0.45-0.52
3	0.50-0.59	0.63-0.69	0.52-0.60
4		0.76-0.90	0.57-0.67
5	0.61-0.68	1.55-1.75	0.60-0.73
6			0.65-0.83
7	0.79-0.89	2.08-2.35	0.72-0.99
8			0.83-1.05

[a]Channel not available when 10-bit infrared data are collected.

Table 2. Comparison of satellite thermal channel characteristics with that of MAMS

	Bandwidth	Central Wavelength	Bandwidth	Central Wavelength	Bandwidth	Central Wavelength
VAS	3.84-4.06	(3.95)	10.36-12.12	(11.17)	12.50-12.82	(12.66)
AVHRR	3.53-3.93	(3.73)	10.34-11.25	(10.76)	11.39-12.33	(11.83)
TM	---	---	10.40-12.50	(11.45)	---	---
MAMS	3.47-3.86	(3.73)	10.55-12.24	(11.12)	12.32-12.71	(12.56)

shorter wavelengths. The 12 μm channel of AVHRR is positioned near 11.8 μm with a bandwidth about twice that of MAMS and VAS (which are centered at longer wavelengths).

The standard MAMS instrument configuration (Table 3) uses the 5.0 mRa aperture and 6.25 rps scan mirror speed. This configuration provides optimal sensing for very high quality thermal measurements. Figure 1 shows the scan geometry for the instrument when flown on the NASA high-altitude aircraft. The dimensions of the ground resolution cell (nominally 100 m at nadir) increase with scan angle from nadir by the $\sec^2(\theta)$. The data are digitized at a fixed angular rate and, with the larger aperture, result in about a 58% (58 m) overlap from one instantaneous field-of-view (ifov) to the next across the scan. The aircraft movement during a scan and from one scan to the next produces an along-track overlap of 66% (66 m) for the FIFE configuration (5.0 mRa aperture, 6.25 rps, 20-km nominal height, and 206 m/s air speed). When the overlapping pixels are all displayed, a somewhat "blurred" scene is available with 58 x 34 m resolution (at nadir). By sub-sampling the data during post-processing, 100 x 100 m non-overlapping contiguous data are available. Interpolation techniques are also used to restore the overlapping data to quasi-independent 30-m resolution data.

MAMS FIFE Data

Two flights were made with MAMS over the FIFE region during Intensive Field Campaign-1 (IFC-1). The first took place during the day of June 4 (1055 - 1154 LDT) and a second on the night of June 5, 1987 (2228-2350 LDT). These times loosely correspond to a period of intense observations by other aircraft and ground-based systems (Sellers et al., 1988). Aircraft restrictions, flight time, and weather conditions limited data collection days and observation times. The flight tracks for these flights are presented in Figure 2. For the June 4 flight, three overpasses were made at roughly 21-min intervals. The passes were made in various directions to measure different reflection patterns from particular regions. For the night flight (June 5), five passes were made at two different angles and directions at approximately 12-min intervals. The different flight directions also allowed for an assessment of thermal emission on view geometry. Details on the MAMS flight tracks and data coverage with respect to the FIFE study region are presented in the Appendix.

The instrument configuration used for FIFE is shown in Tables 1 and 3. For the FIFE flight of June 4, the visible channel gains were set so that saturation did not occur over bright scenes. As a result the channel sensitivity approached that of the quantization level which is a function of the channel calibration constant (or

Table 3. Standard MAMS instrument configuration

Scan speed	6.25 rps
Instantaneous field-of-view (ifov)	5.0 mRa
Ground resolution @ 20 km	100 m at nadir
Total field-of-view (fov)	85.92°
Swath width @ 20 km (agl)	37.2 km
Spectral bands	7 visible/near infrared[a]
	3 thermal infrared[b]
Roll correction	±15.0°
Pixels per scan line	716
Calibration sources	2 controlled blackbodies
Digitization	8 bits (vis), 10 bit (IR)

[a]One visible channel is lost when 10-bit thermal data are collected
[b]A redundant fourth channel may be selected with a different gain setting

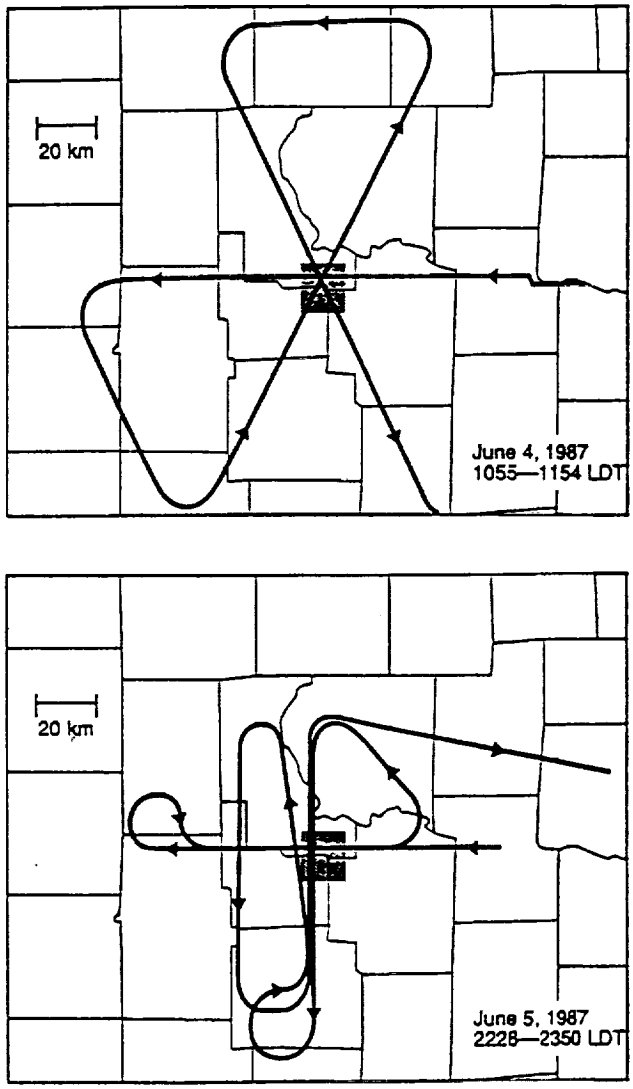


Figure 2. MAMS flight tracks over the FIFE study region.

instrument gain). These values are presented in Table 4. Random noise estimates were made for the FIFE imagery based on structure function analysis (Hillger and Vonder Haar, 1988). Extrapolation of the structure function curves to zero (or small) separation distances allows an estimate of the random noise in a scene. This technique has advantages over more traditional variance methods in that it is not strongly biased by natural gradients in the scene. For the visible channels, signal-to-noise values ranged from 20 to 70 for land scenes, with the highest values in channel 7.

The 3.7 μm channel was used in place of the 6.5 μm channel for FIFE. This provided additional information on the surface thermal and emissivity characteristics. The 3.7 μm channel was also selected as the redundant infrared channel available on the Daedalus systems, and the gains were set such that better sensitivity was available with channel 9 than with channel 10. A modification to the digitizer allowed for the infrared channels to be collected with 10 bits of resolution with channel 1 (0.42-0.45) becoming the "bit bucket" for the two least significant bits from the four infrared channels (Jedlovec et al., 1989). Ten-bit sensitivity values for these channels are shown in Table 4. All four of the infrared channels were quite sensitive to small temperature changes with sensitivity values less than 0.1 K. The dynamic range extended from 240-325 K for channels 9, 11, and 12 and up to 345 K for channel 10. This range encompassed the observed brightness temperatures (not land surface temperature) of the FIFE observations.

The accuracy of MAMS infrared data has improved since its development as refinements to the instrument and calibration procedures were made (Jedlovec et al., 1989). Thermal data from both FIFE flights are of very high quality. NEDT estimates (determined from structure analysis) are equal to or less than the quantization levels (Table 4). The relative accuracy of the temperature fields mapped by MAMS has been shown to be very good. Thermal gradients in skin and sea-surface temperature derived from MAMS data match precisely those derived from AVHRR channel measurements and in situ observations (Jedlovec et al., 1989; Moeller et al., 1989). Absolute accuracy is less certain and may range up to ± 4 K depending on the type of data used in the comparison (Jedlovec et al., 1986a, 1989).

Table 4. Channel sensitivities and single sample noise estimates for MAMS channels for FIFE on June 4, 1987

Channel	Central Wavelength	Gain (G)	Calibration Value (X)	Sensitivity (unit/count)	NEdR (land)	S/N	NEdR (water)	S/N
2	0.485	2.0	0.1076	0.0538	<0.1076	>60	<0.0538	>70
3	0.560	1.0	0.1000	0.1000	<0.1000	>30	<0.1000	>30
4	0.620	1.0	0.1225	0.1225	<0.1225	>20	<0.1225	>30
5	0.660	1.0	0.0688	0.0688	<0.0688	>40	<0.0688	>40
6	0.720	0.5	0.0500	0.1000	<0.0500	>50	<0.1000	>20
7	0.805	0.5	0.0354	0.0708	<0.0354	>70	<0.0708	>20
8	0.940	0.5	0.0255	0.0510	<0.0255	>70	0.0024	>10

Channel	Central Wavelength	Sensitivity (unit/count)		Single Sample Noise			
		Radiance	Temperature	NEdR	(R)	NEDT	(T)
9	3.730	0.0025	0.093	0.0001	0 .648	0.360	296
10	3.730	0.0048	0.165	<0.0048	0 .648	<0.165	296
11	11.120	0.1221	0.075	<0.1221	126.391	<0.075	296
12	12.560	0.1533	0.093	<0.1533	129.385	<0.075	291

CALIBRATION

Unlike low- and middle-altitude research aircraft, the high-altitude U2 does not allow for direct interaction with any scientific instrumentation during a flight. In-flight calibration data are not available for the visible channels. Therefore, raw data in the visible channels are converted to radiance units based on pre- and post-flight calibration data with a known light source. The visible channel calibration values can change from one series of flights to another for a number of reasons. The infrared calibration procedure used for the FIFE data is similar to that presented in Jedlovec et al. (1989). The following two sections provide a detailed explanation of the visible and infrared calibration procedures.

Visible Channels

Prior to each instrument flight, the gain for each visible channel is set to optimize channel sensitivity and dynamic range for that flight. Gain values from previous flights are used as initial input and are adjusted accordingly, to cover the expected range of scene reflectances. The analog-to-digital processing of the MAMS data during flight converts the dc restored channel voltages to 8-bit raw count values which are recorded on magnetic tape. Visible channel data require post-processing to convert raw counts into radiance values.

Since both scene and calibration data values are based on the performance of the entire optical system, instrument component degradation (as a function of time) may affect the measured radiance values. Probably most significant is the buildup of a film (dirt) on the surface of the scan mirror. Since the scan mirror is exposed to the environment throughout the flight, haze, atmospheric aerosols, and water vapor contribute to the buildup of this film on the scan mirror. Because of the lack of internal visible calibration on MAMS, the effect of this buildup is not known. The resulting degradation of the signal is most significant at longer near infrared wavelengths (Jeff Myers, NASA-Ames, personal communication). Therefore, in order to obtain accurate visible channel data, periodic calibration with an integrating sphere, and careful scan mirror cleaning is required. For the data collected during the FIFE flights, calibration values from a May 1987 laboratory calibration were used to convert raw counts to radiances. Post-deployment calibration using an integrating sphere (July 1987) did not show any significant difference from pre-deployment values.

Visible calibration values were determined in the laboratory with the MAMS viewing a constant light source from an integrating sphere. The intensity of the light

from the sphere is accurately known in 10-nm increments throughout the visible and near infrared portion of the spectrum. The integrating sphere itself was calibrated against Bureau of Standards precision instrumentation. The relationship of the observed versus known intensity values was modeled based upon the spectral response characteristics of the MAMS visible channels. The resultant calibration values, $X(\iota)$, for the $\iota = 2$, 8th visible channel, were used to convert flight data to radiance units using

$$\Re_{vis}(\iota) = C_{raw}(\iota)\, X(\iota) / G(\iota) \tag{1}$$

where $\Re_{vis}(\iota)$ is the calibrated radiance, $C_{raw}(\iota)$ the raw count value, $X(\iota)$ the calibration value (from pre/post-flight calibration), and $G(\iota)$ the gain in the ι-th visible channel. The channel gains and calibration values for the FIFE flights are presented in Table 4.

Infrared Channels

The MAMS views a warm and a cold blackbody of known temperature every spin (6.25 times per second). The blackbody temperatures are selected to encompass the expected scene temperatures. Since the instrument response and infrared calibration are highly linear in terms of radiances (Menzel et al., 1986), it is necessary to convert known blackbody temperatures to channel radiances for application to the infrared scene data. The upwelling radiance from the scene or blackbody, $\Re_{ir}$, determined by MAMS in a particular channel with a temperature, T_s, is given by the convolution of the channel spectral response $\psi(\nu)$ and the Planck radiance, β, in the radiative transfer equation as

$$\begin{aligned}\Re_{ir} = & \int_{\nu_1}^{\nu_2} \epsilon(\nu)\,\beta(T_s,\nu)\,\tau(\nu)\,\psi(\nu)\,d\nu \;/\; \int_{\nu_1}^{\nu_2} \psi(\nu)\,d\nu \\ & + \int_{\nu_1}^{\nu_2} \int_{P_0}^{P_s} (1-\epsilon(\nu))\,\tau(\nu)\,\beta(T(p),\nu)\,\psi(\nu)\,d\tau(p)\,d\nu \;/\; \int_{\nu_1}^{\nu_2} \psi(\nu)\,d\nu \\ & - \int_{\nu_1}^{\nu_2} \int_{P_0}^{P_s} \beta(T(p),\nu)\,\psi(\nu)\,d\tau(p)\,d\nu \;/\; \int_{\nu_1}^{\nu_2} \psi(\nu)\,d\nu \end{aligned} \tag{2}$$

where τ is the path atmospheric transmittance, ϵ is the surface emissivity, and ν represents the wavenumber. The first term on the right-hand side represents the upwelling radiation from the surface, the second term the downwelling radiation from

the atmosphere reflected to the instrument by the surface, and the third term is the upwelling radiation from the atmosphere. When viewing the instrument blackbodies $\epsilon = 1$, and the atmosphere effect between the scan mirror and the blackbodies is negligible making $\tau = 1$, and $d\tau = 0$. Therefore, (2) becomes

$$\Re_{ir} = \frac{\int_{\nu_1}^{\nu_2} \beta(T_{bb},\nu)\psi(\nu)d\nu}{\int_{\nu_1}^{\nu_2} \psi(\nu)d\nu} \tag{3}$$

which still requires integration over the spectral response function. For easier blackbody radiance determinations, (3) is approximated by

$$\Re_{ir} \approx \beta(T_{bb},\nu_o) \tag{4}$$

where ν_o is the half power wavenumber defined by

$$\nu_o \equiv \frac{\int_0^{\nu_o} \psi(\nu)\delta\nu}{\int_0^{\infty} \psi(\nu)d\nu} = 0.50 \tag{5}$$

This half power wavenumber best represents the asymmetric characteristics of the spectral response curve. When ν_o is used in (4), the Planck function β approximates the energy in a MAMS channel for a given temperature T. Since the Planck function peak (maximum emission) shifts (with respect to wavelength or wavenumber) with changing scene temperature, a correction to the half power wavenumber is necessary. This monochromaticity correction is more conveniently applied to the temperature in (4) than to the wavenumber and is calculated by forming linear relationships between ν_o and T over a typical range of scene temperatures. This application produces corrections in each channel given by

$$T^c_{bb} = (T - \alpha_2) \; / \; \alpha_1 \tag{6}$$

so that an improved expression becomes

$$\Re^{c}_{ir} \approx \beta(T^{c}_{bb}, \nu_o) \tag{7}$$

where α_1 and α_2 are linear regression coefficients. Values for the half power wavenumbers and the temperature correction coefficients are listed in Table 1. Equation (7) is only used in the calibration equations presented below; otherwise, the more rigorous equation (2) is used.

Raw infrared count values from the scene were related to the energy received by the detectors through an assumed linear response given by

$$\Re_{ir}(\iota) = b(\iota) + m(\iota)\, C(\iota) \tag{8}$$

where $\Re_{ir}(\iota)$ is the calculated radiance, $C(\iota)$, the raw count value, and ι is the infrared channel designator. The blackbody radiances $R_{bb}(\iota)$, and the corresponding counts, $C_{bb}(\iota)$, form calibration curves for the MAMS channels. Calibration was performed for each channel separately for every scan line. Values $m(\iota)$ and $b(\iota)$ are the slope and intercept of the infrared channel calibration curves.

NAVIGATION

Navigation of flight data was performed for segments of flight tracks which are straight lines. For these segments aircraft navigation parameters (latitude and longitude) can be fit to linear functions with small residual errors. Navigation is used for the selection of data segments, and the remapping of scenes to common map projections for comparisons. Universal Transverse Mercator (UTM) and rectilinear projections have been used for the MAMS FIFE data.

Data Sources

The aircraft inertial navigation system (INS) measured the aircraft position and attitude. The parameters are recorded by the INS system every five seconds, or an average of every 31.25 scan lines at 6.25 scans per second. The position parameters were latitude, longitude, and altitude, while the attitude parameters were pitch, roll, and heading. The aircraft roll does not affect the scene data since it is automatically compensated for by the timing of the digital data recording in the instrument. The INS latitude and longitude readings were used to plot the flight tracks on a map base, with time tags at specified intervals (as in Figure 2 and in Figure A1 of the Appendix). Examination of these plots for various time intervals allowed the selection of preliminary beginning and ending times for the extraction of scene data.

For straight line flight tracks the aircraft latitude and longitude are defined by linear functions in time. Each parameter requires two coefficients: the initial value (intercept) and the rate of change (slope). These are determined by linear regression over the time period corresponding to the image. In the Man-computer Interactive Data Access System (McIDAS) the coefficients are stored as ancillary data for each image.

In some sections of the data tape, scan lines were not recoverable during the transfer of data from the aircraft recorder tape to Computer Compatible Tape (CCT) as a result of bit losses in the deconvolution system (Jeff Myers, NASA-Ames, personal communication). Gaps in the data must be filled in order to preserve the geometry of the scene for navigation. During data extraction from the CCT, the occurrence of a missing data line was detected by a gap in the scan line numbers which are part of the documentation header for each line. If the expected scan line number was not read, a fill line was generated. Fill lines were generated by using the expected scan line number, the calibration information from the previous good line, and linear interpolation of the data values between the surrounding two adjacent good lines, which is tolerable because of the along track overlap from one line to the next.

For data losses greater than several lines, a gap of zero values was left in the image.

Corresponding image and navigation segments are extracted by the time tags in each data stream. For the data of June 4 the navigation error was greater than expected from instrument drift, especially along the flight track. It was discovered that the MAMS and INS clocks differed by slightly over 3 minutes. Since the aircraft roll angle is recorded by both systems, the time difference can be determined by matching roll variations. Plots of roll data from the first FIFE flight are given in Figure 3 and show the time difference of approximately 3 minutes (0.05 hour). This problem occurred temporarily because the MAMS clock was being set manually. An interactive program was used to vary the time bias until the two plots matched.

The Algorithm

The Earth location of a MAMS pixel was found by first determining the elapsed time from the beginning of the scene. The aircraft subpoint latitude and longitude were determined from the linear fit equations. The scanner angle (DD) was obtained from the data element location in the scan line and the angular distance per element (Figure 1). The distance (D) from the aircraft subpoint to the data element was the aircraft altitude multiplied by the tangent of the scanner angle. The direction of the scan line is always at right angles to the current heading. The spherical triangle formed by the scan line and the latitude lines through the pole was solved by the laws of sines and cosines to determine the Earth coordinates of the image point.

An inverse navigation transform was used to determine image coordinates from Earth coordinates. The algorithm was initialized with the input Earth location, starting aircraft subpoint, and the direction of the flight track. Along with the scan line through the input point perpendicular to the flight track, these parameters defined a right triangle in the image (Figure 1). In this triangle, the distance along the track and hence the elapsed time were obtained. The aircraft heading at this time was used to rotate the scan line so that it is perpendicular to the heading. The aircraft nadir point and elapsed time were adjusted accordingly. The scan rate and the elapsed time were used to compute the number of scan lines to the input point. The distance along the scan line was used to compute the element number.

Navigation Correction Using Landmarks

The correction technique for error and drift in the INS measurements evolved using the eight FIFE overpasses. Once the navigation fit parameters have been computed as a function of time, each point in the image can be Earth located. Earth location values for landmarks identified in the scene were obtained to give a coarse

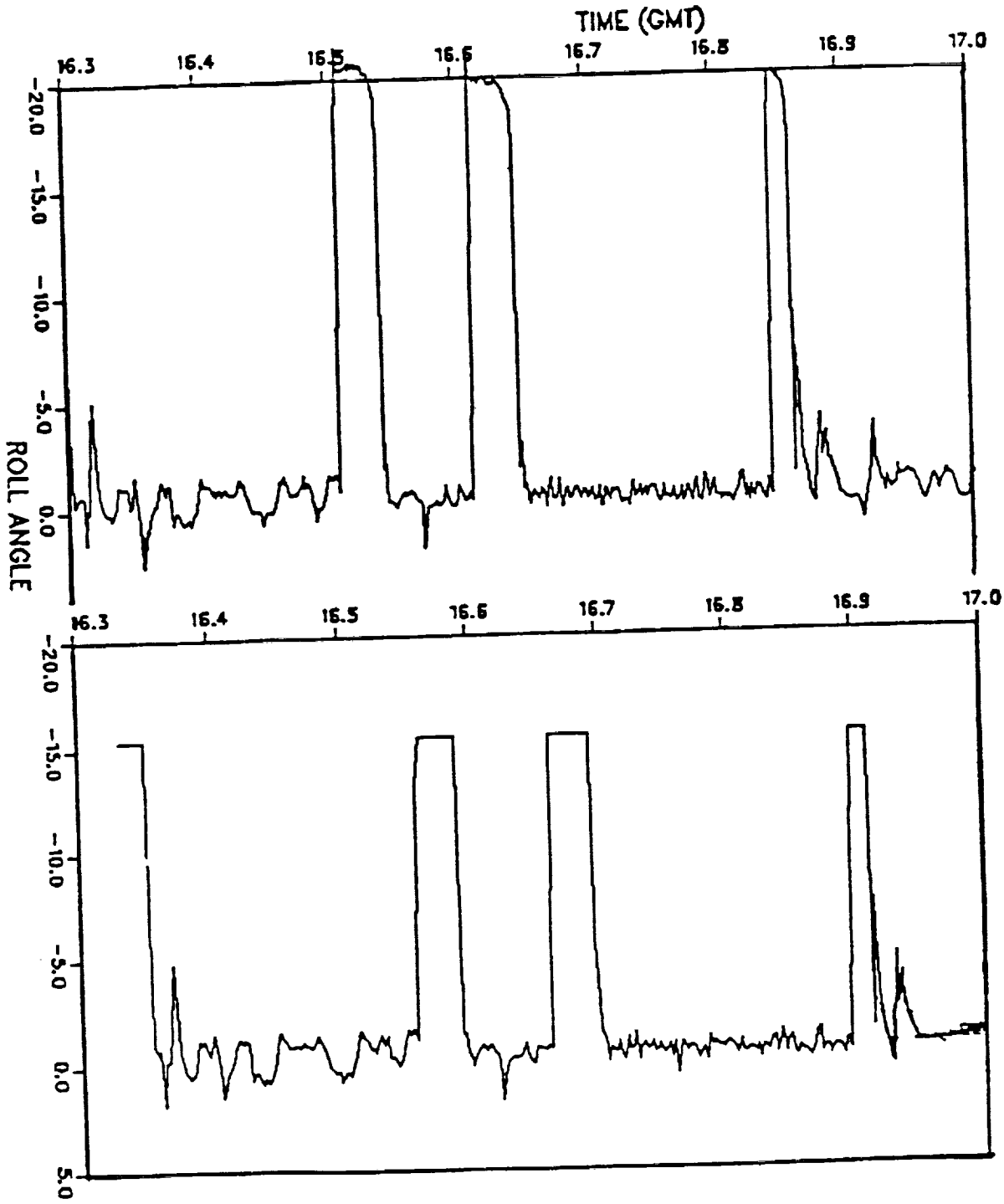


Figure 3. Aircraft roll data from INS and MAMS data streams.

estimate of the navigation accuracy. During the several hours of flight time, INS navigation readings typically show an accumulated drift of a few kilometers, which was apparent from a displacement in the location of landmarks in the imagery. The FIFE scenes have an excellent central landmark which is the intersection of Interstate 70 and Kansas Highway 177. For the first pass, with a heading of due west, the coordinates of the intersection were in error (i.e., translated) by 110 scan lines. The calculated navigation coordinates at this position were corrected by solving two equations for the corrections to the constant terms in the linear regression fits. The images also showed rotations in some regions, due to the drift in the latitude and longitude INS values during the elapsed time of a scene. This was reduced by adjusting the slope coefficients of the regression fits and requires, at a minimum, a second landmark in order to correct the second regression coefficient.

This method was found to be overly sensitive to the choice of the second landmark, resulting in large adjustments to the slope coefficients, and navigation was not improved at locations away from the landmarks. These results indicated that a distribution of landmarks over the image was required. U. S. Geological Survey (USGS) 7.5-minute (1:24,000 scale) topographic maps covering the FIFE site were used to locate landmarks in Earth coordinates. The image locations were read from magnified image displays centered on each of the landmark coordinates. For the daytime images both visible and near infrared channels were used for identifying landmarks, while only infrared images could be used at night. The latter had only slight impact on registration accuracy. Thirty landmarks were located and the adjustments were calculated by multiple linear regression. The adjustments to intercepts and slopes are typically a few minutes of arc.

Although the latitude/longitude INS errors are small, the magnitudes of the adjustments can be better understood relative to the MAMS resolution of 100 m, which is approximately 0.001°. For the first pass, with heading due west, the along track (longitude) error at the I70-177 intersection is 0.0419° (or 2 minutes 31 seconds). In ground distance, at a latitude of 39.1°, this error is 0.0419° X 111 km/deg X COS(39.1) = 3.6 km. This distance in scan lines, which are separated by 33 m, is 3.6/0.033 = 110 lines.

The INS parameter which has the largest impact is heading, since it typically has variations of a few degrees, and one degree corresponds to 300 m at the extremes of a scan line. Since a large number of landmarks and flight segments were available, a study was undertaken to determine the correlation between INS measurements and landmark errors. In the case of the FIFE data, the INS heading values were missing. Therefore, heading values were derived from the aircraft velocity components, which were available. These values will be referred to as the INS heading values. For each

landmark, the aircraft position was found from the elapsed time (based on scan lines) and the regression fits. Then, the aircraft heading that would actually place the landmark in the scanner's field of view was calculated. These headings were plotted and compared to the INS values as shown for selected passes in Figure 4. The variations in the two values are similar, although at times they are displaced, indicating a bias in the INS readings. The correlation indicates the importance of accurately representing the INS readings in the navigation calculations.

Consequently, two additions were made to the navigation process. The least squares fits to altitude, heading, and pitch were expanded to include a quadratic term, and their intercepts and slopes were corrected by applying multiple linear regression to the landmark points. The headings determined from the corrected intercepts and slopes and landmark-derived headings are shown in Figure 5. The root mean square (RMS) errors in the landmark coordinates (pixels) are given in Table 5.

An additional requirement for obtaining the most accurate fits is the removal of spurious and missing readings for aircraft pitch. Missing readings in the character values are interpreted as zero. The occurrences of these spurious and missing points, and the fits obtained when they are ignored, are shown in Figure 6.

Navigation Correction During Remapping

For both the day and night FIFE data, the overlapping images were remapped to a UTM projection with 30-m spacing between pixels. Remapping to a new map projection involves the moving of input pixels to their proper locations in the output image. The remapping process requires stepping through the image coordinates of the remapped output image, computing the Earth coordinates, and then computing the corresponding image coordinates of the input image. The input pixel values are then placed in the output image. This process requires two navigation transformations at each coordinate, which is computationally time consuming. The McIDAS remapping program uses a spline technique in which the navigation computations are performed by default at 20-pixel intervals and linearly interpolated in between.

After remapping, navigation discrepancies were apparent as shifts between the images. A plot of the displacements at 16-pixel intervals between the first two passes over FIFE is shown in Figure 7. The largest displacements are around 6 pixels, which can occur when the maximum navigation errors of three pixels are additive. A technique was developed using a modified version of the Marshall Space Flight Center (MSFC) automated winds routine (Wilson, 1984) to measure the residual shifts and then remove them during the remapping. The residual errors in remapped images were measured using template matching. Since the displacements between remapped

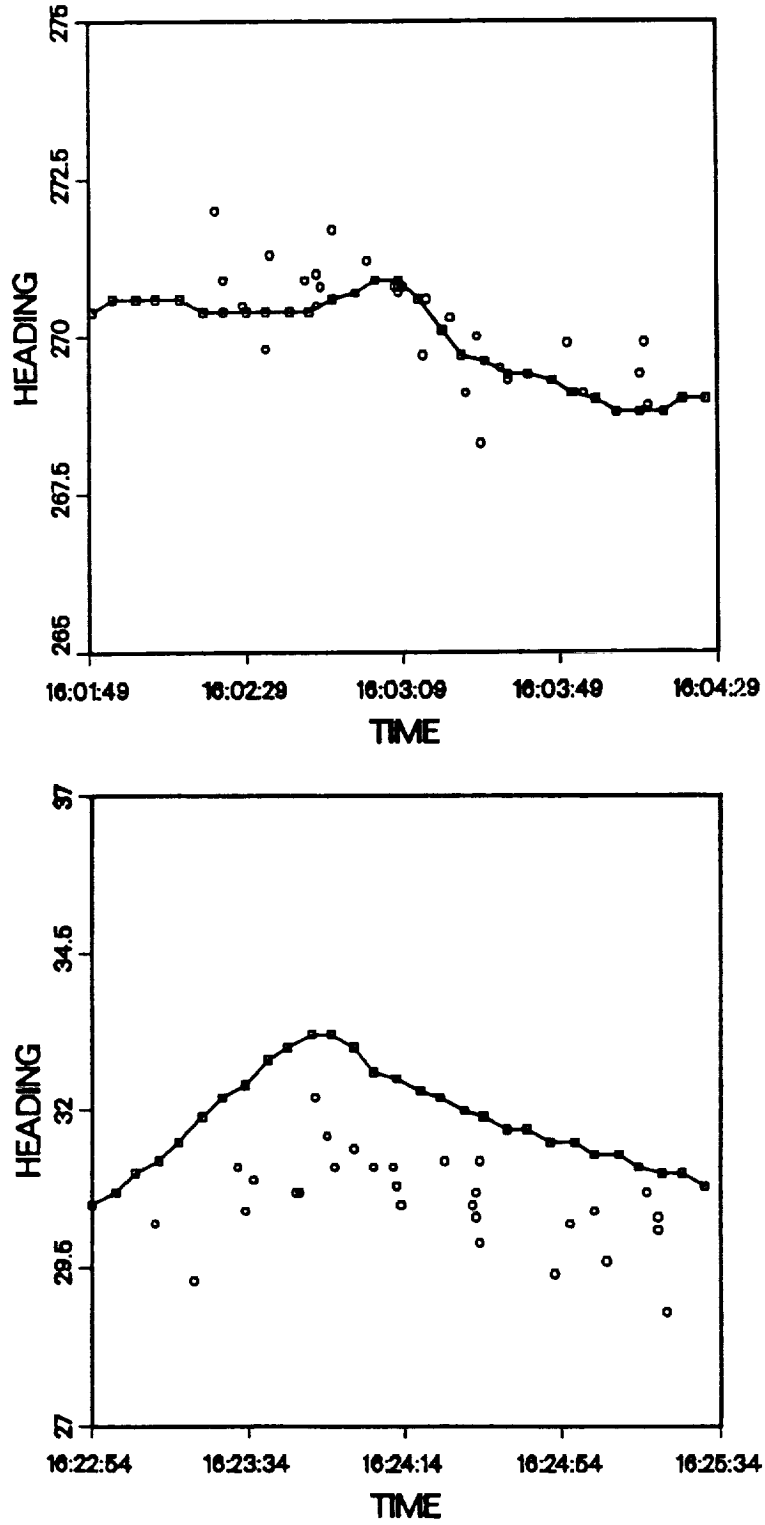


Figure 4. Landmark-determined (points) and INS (line) headings.

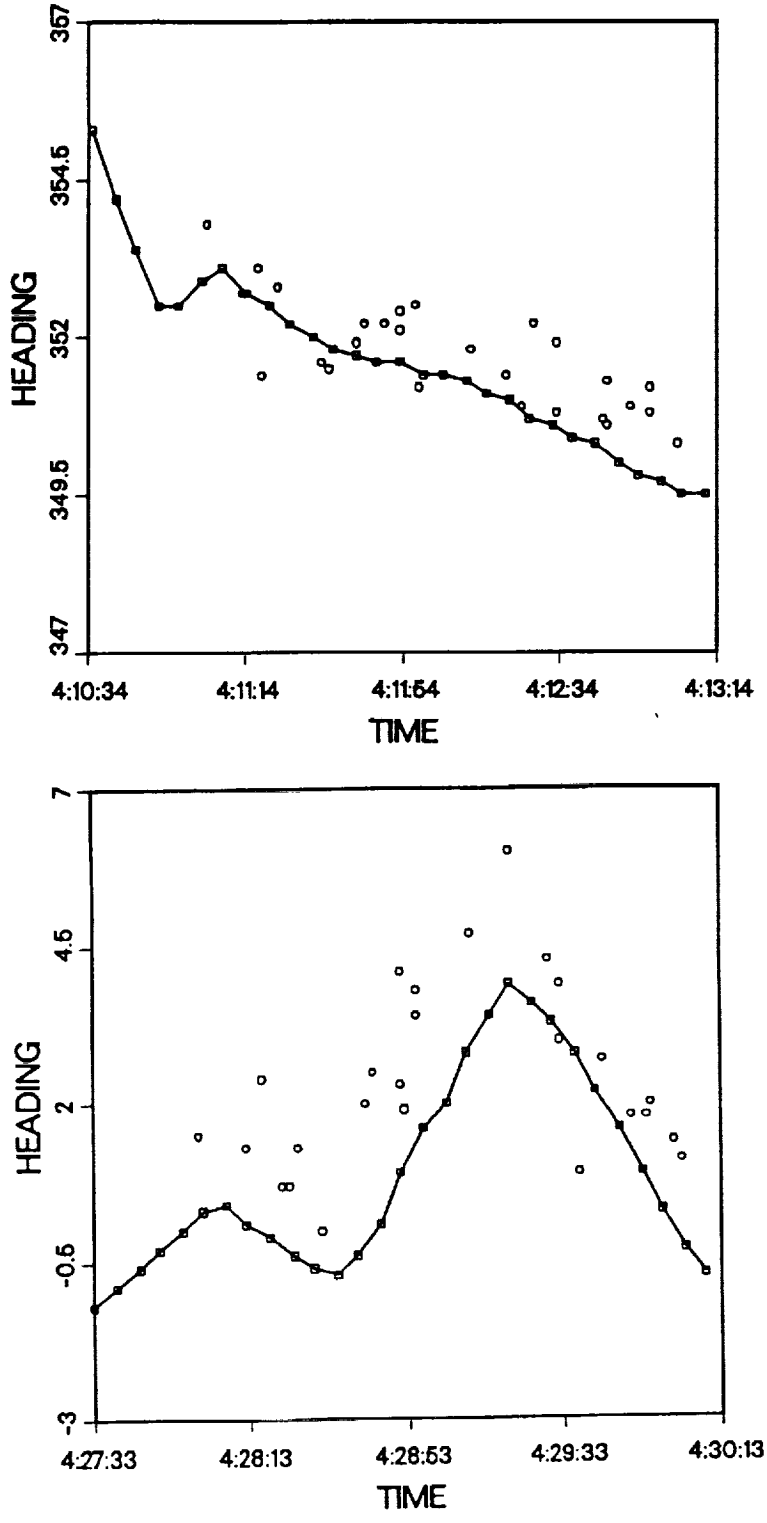


Figure 4. (Continued)

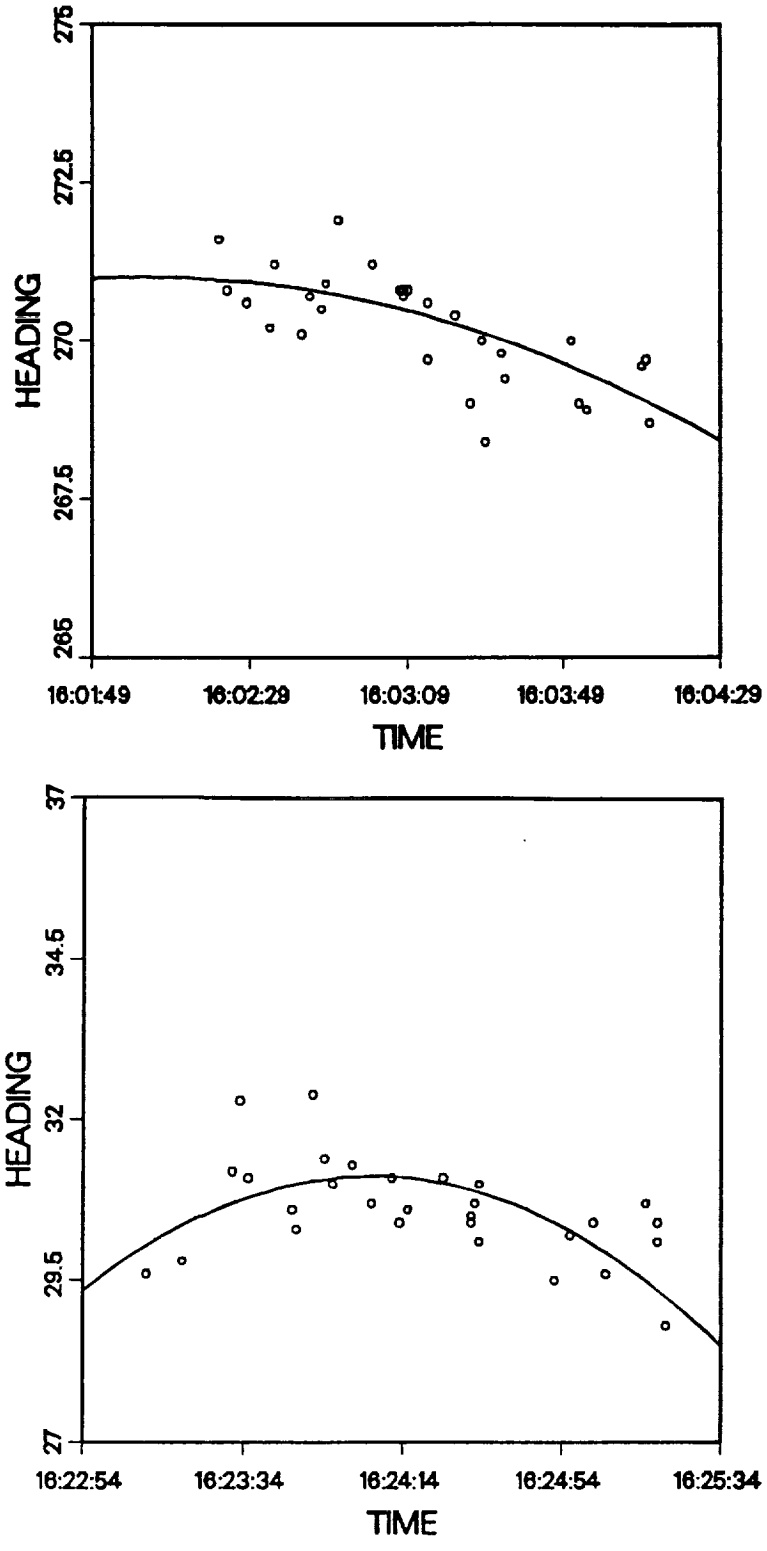
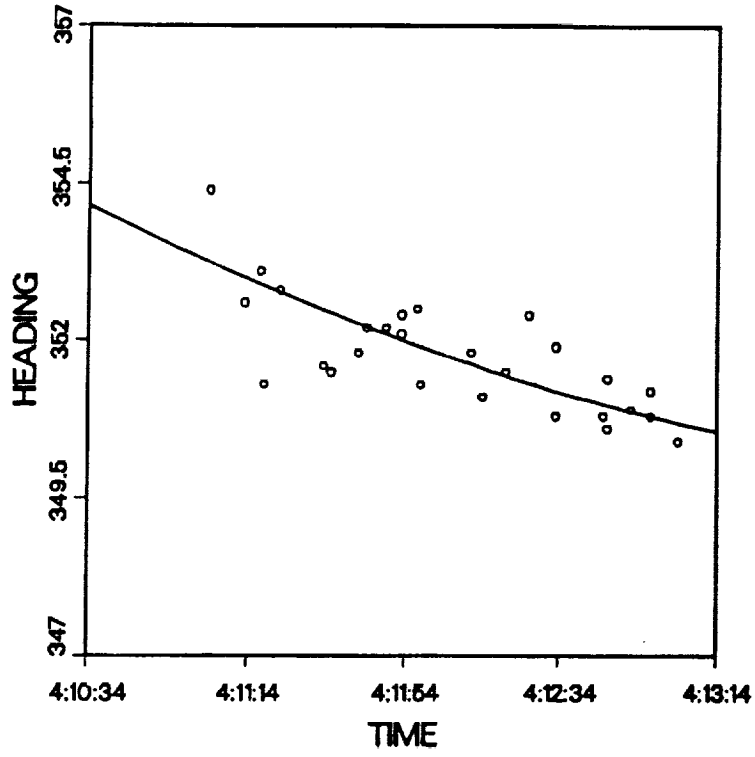


Figure 5. Landmark-determined headings and corrected regression fit of headings.



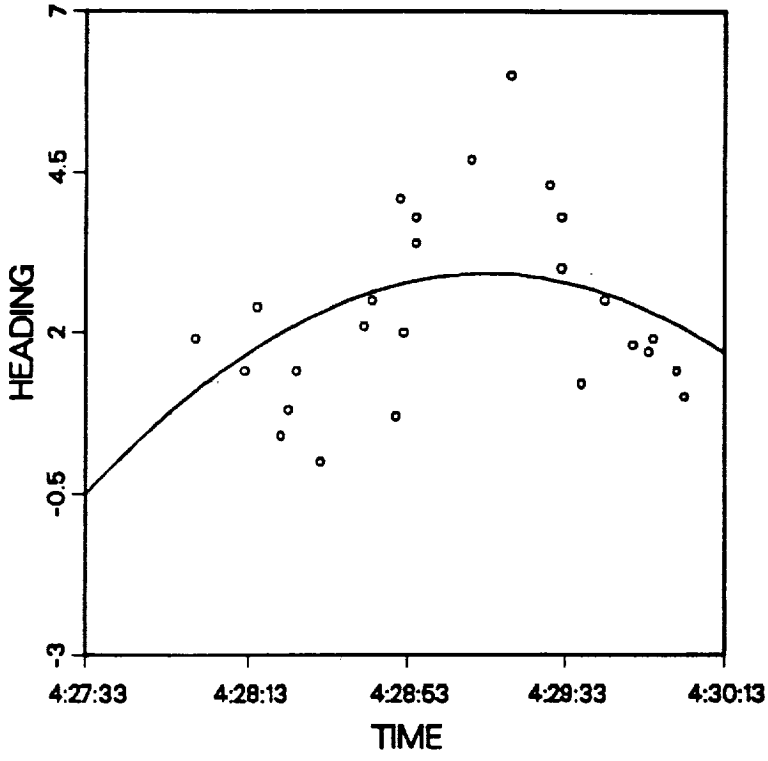


Figure 5. (Continued)

Table 5. Landmark RMS errors (pixels)

Pass	Source of INS Values				
	INS Alt/Pitch/Hdg with Interpolation	Linear Fit		Quadratic Fit	
		Lat/Lon Corrected	Lat/Lon, Alt/Pitch/Hdg Corrected	Lat/Lon Corrected	Lat/Lon, Alt/Pitch/Hdg Corrected
1	1.87	2.48	2.00	2.17	1.87
2	4.46	3.40	1.92	4.32	1.75
3	2.12	2.82	2.69	2.30	1.96
4	3.90	3.72	1.98	3.84	1.89
5	3.02	2.41	1.84	2.75	1.81
6	2.37	2.76	2.45	2.37	2.10
7	3.34	3.13	2.45	3.15	2.32
8	5.19	5.76	4.56	4.78	3.75

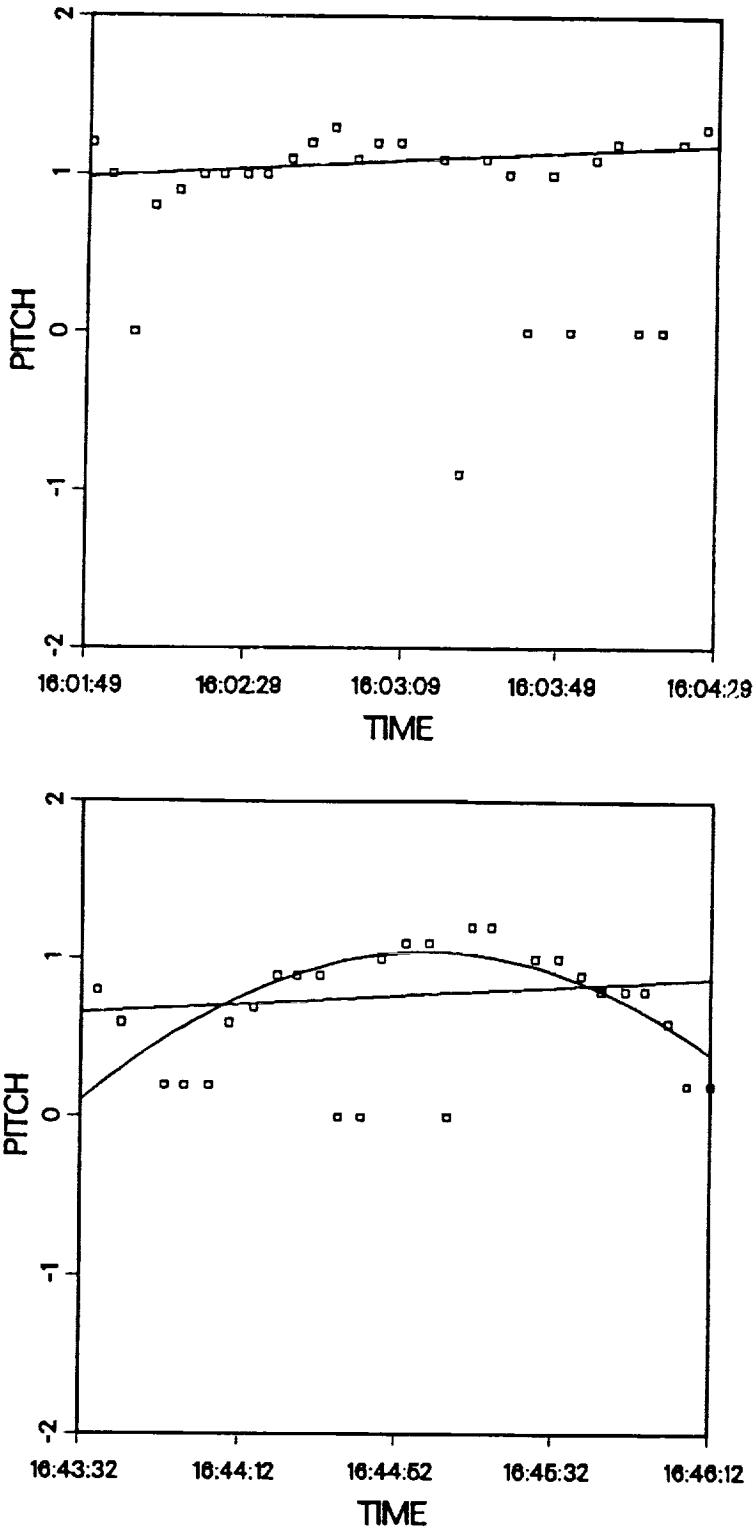


Figure 6. Regression fit of pitch with spurious readings ignored.

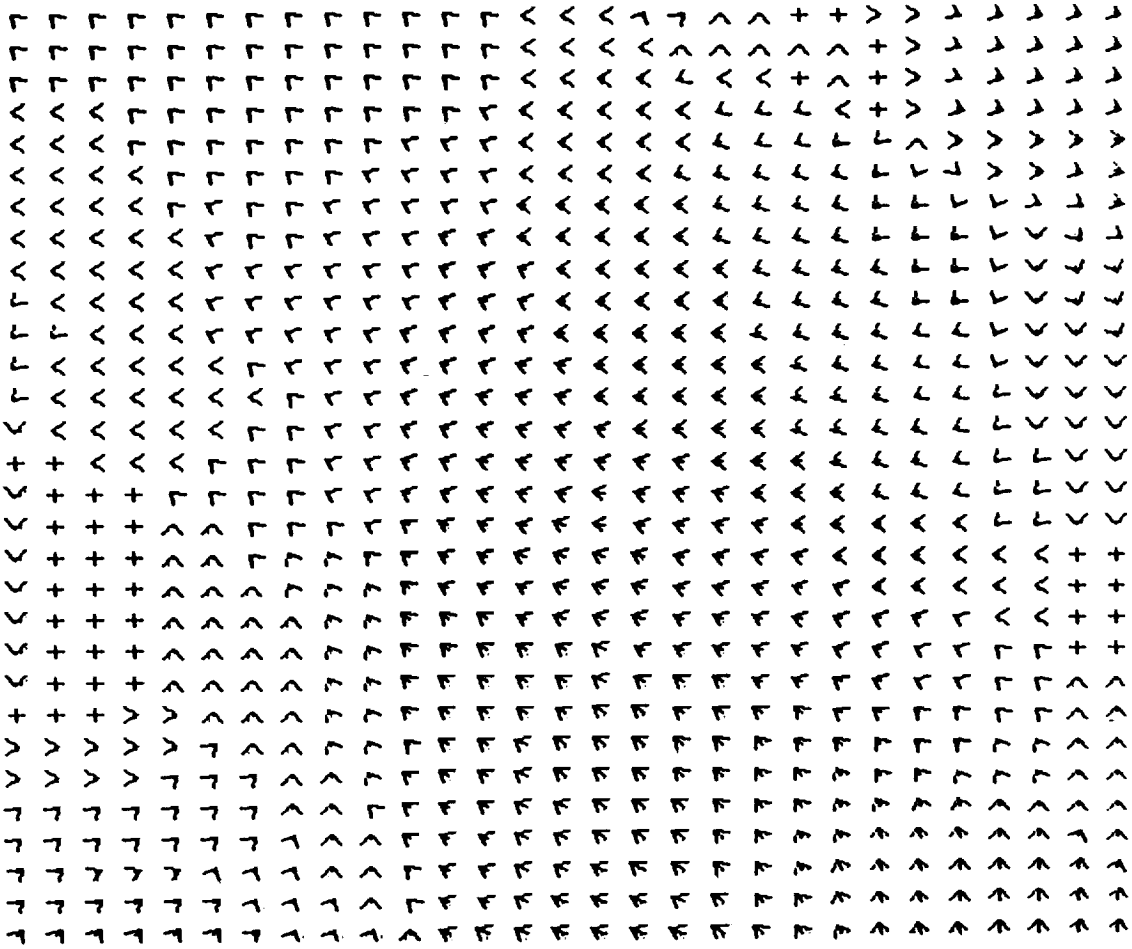


Figure 7. Displacements after remapping FIFE passes 1 and 2 into UTM coordinates, where the length of the arrow indicates the displacement.

images are slowly varying spatially, large templates of 75 pixels on a side were used. The residual errors between remapped images were measured at 16-pixel intervals. Displacements near the edges where the template cannot be moved were obtained by using images larger than the final remapped products. Some editing of incorrect displacements was done. The displacements were averaged so that the remapped images were corrected to a common location. In the remapping program, the displacements were removed from the output image coordinates before computing the input image coordinates. This process puts the input pixels at remapped positions without the displacements, and residual shifts are no longer apparent. ***The resulting images from this procedure were co-registered to within one pixel over most of the study region for both day and night data.***

Universal Transverse Mercator (UTM) Grid System

The Universal Transverse Mercator projection and grid system has widespread application, including the FIFE Information System (FIS) (Sellers et al., 1988). Beginning in 1977, many USGS maps have used this system, replacing the Polyconic projection. Since it can be adapted for any region by defining a new axis, it is used by many countries for topographic mapping and military maps, including the U.S. Army since 1947. Maps of other planets and moons have also been generated in the UTM coordinate system beginning in 1927.

The standard Mercator projection is defined geometrically by a cylinder wrapped around the globe in contact with the equator. The Earth's features are projected onto the cylinder, which is then cut at some point and laid out flat to form the map. Longitude lines become parallel, rather than converging at the poles, and latitude lines become spaced farther apart to compensate for the spread in longitude lines. Thus, angles and local scales are preserved so that a constant azimuth line is straight. This is the conformal property, and the line is called a loxodrome or rhumb line. Thus, the Mercator projection is useful for navigation. The transverse Mercator projection is generated by rotating the cylinder by 90° so that a longitude line becomes the tangent or contact line, and a north-south strip is mapped very accurately. The agreement between the cylinder and the globe can be increased by using a secant cylinder, which is slightly less in diameter than the globe and so intersects it in two places within the strip. The geometry of the projection is shown in Figure 8 (Greenhood, 1964).

Since the secant cylinder lies below the surface of the globe at the zone centers, the scale is reduced by a factor of 0.9996 relative to the scale at the intersections of the cylinder and the globe, which are 180 km from the zone centers. Scale variation over a UTM zone is no more than 1 part in 1000 when an ellipsoid Earth model is

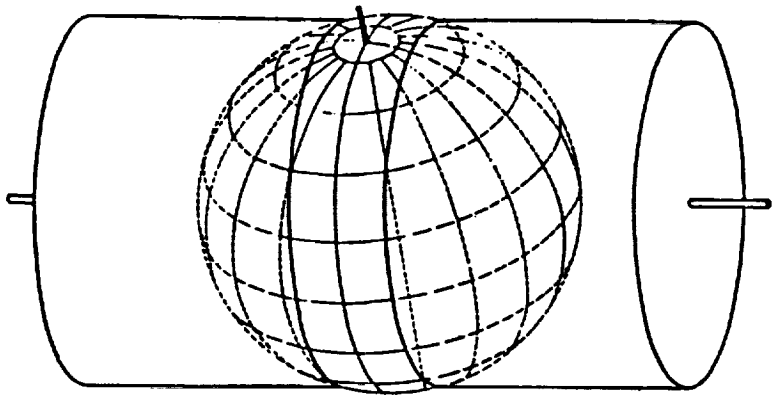


Figure 8. Transverse Mercator projection geometry (after Greenhood, 1964).

used. For U.S. maps the Clarke 1866 ellipsoid is used. The UTM system divides the world into 60 zones of 6° width which are numbered starting at 180° longitude and increasing to the east. The U.S. zone numbers range from 10 on the west coast to 19 on the east coast. The equator is assigned a value of 0 meters north, and the central meridian is assigned a value of 500,000 meters east in order to avoid negative numbers.

Projection Formulas

Formulas are used to transform from latitude and longitude values to UTM coordinates in meters. Accuracy to within 1 meter can be obtained only by using a realistic model for the Earth, which is very nearly an ellipsoid of revolution with a flattening of about one part in three hundred. The Clarke 1866 ellipsoid has an equatorial radius (a) of 6,378,206.4 meters and a polar radius of 6,356,583.8 m. The flattening is then 1 / 294.98 and the eccentricity (e) is 0.082272. Distances on the ellipsoid are typically calculated by integration of expressions in latitude and longitude, which may require expansion in series before integration (Pearson, 1990).

The easting distance from the central meridian is, to first order, the product of the scale (k, where k = 0.9996), the radius of curvature of the ellipsoid parallel to latitudes (N), the longitude difference in radians, and a latitude cosine factor for the reduced spacing of the meridian lines.

$$\begin{aligned} x &= kN(\lambda - \lambda_o)\cos\phi \\ &= kNA \end{aligned} \tag{9}$$

where,

$A = (\lambda - \lambda_o) \cos \phi$, with λ and λ_o in radians.

The northing distance along a meridian on the ellipsoid is to the first order, the product of radius and latitude in radians, $a\phi$. As a function of latitude and eccentricity, integrated over the latitude range, the resulting series is

$$\begin{aligned} M = a[&(1 - e^2/4 - 3e^4/64 - 5e^6/256 - \ldots)\phi - (3e^2/8 + 3e^4/32 \\ &+ 45e^6/1024 + \ldots)\sin 2\phi + (15e^4/256 + 45e^6/1024 + \ldots)\sin 4\phi \\ &- (35e^6/3072 + \ldots)\sin 6\phi + \ldots] \end{aligned} \tag{10}$$

For the Clarke 1866 eccentricity constant, the series can be evaluated as:

$$M = 6{,}367{,}399.69\phi^r - 16216.94\sin 2\phi + 17.21\sin 4\phi - 0.02\sin 6\phi \qquad (11)$$

The expressions corrected for higher order terms in latitude and longitude are as follows:

$$\begin{aligned} x &= kN[A + (1 - T + C)A^3/6 + (5 - 18T + T^2 + 72C - 58e'^2)A^5/120] \\ y &= k\{M + N\tan\phi[A^2/2 + (5 - T + 9C + 4C^2)A^4/24 \\ &\quad + (61 - 58T + T^2 + 600C - 330e'^2)A^6/720]\} \end{aligned} \qquad (12)$$

where,
$e'^2 = e^2/(1 - e^2)$
$N = a/(1 - e^2 \sin^2 \phi)^{1/2}$
$T = \tan^2 \phi$
$C = e'^2 \cos^2 \phi$

For the inverse equations, the latitude is, to first order, called the rectifying latitude (μ), and is 90 degrees times the ratio of the distances from the equator to the input point (M) and to the Pole. The distance (M) along a meridian is given above as a series in eccentricity and actual latitude, and after evaluation with Clarke constants. Inverting the equation for μ, as a function of ϕ, gives the latitude at the central meridian in terms of eccentricity and μ:

$$\begin{aligned} \phi_1 &= \mu + (3e_1/2 - 27e_1^3/32 + \ldots)\sin 2\mu + (21e_1^2/16 - 55e_1^4/32 + \ldots)\sin 4\mu \\ &\quad + (151e_1^3/96 - \ldots)\sin 6\mu + (1097e_1^4/512 - \ldots)\sin 8\mu + \ldots \\ &= \mu + 2.5468693X10^{-3}\sin 2\mu + 3.7839708X10^{-6}\sin 4\mu \end{aligned} \qquad (13)$$

The latitude away from the central meridian is corrected by a series of terms which are second order and above in the easting value:

$$\begin{aligned} \phi &= \phi_1 - (N_1\tan\phi_1/R_1)[D^2/2 - (5 + 3T_1 + 10C_1 - 4C_1^2 - 9e'^2)D^4/24 \\ &\quad + (61 + 90T_1 + 298C_1 + 45T_1^2 - 252e'^2 - 3C_1^2)D^6/720] \end{aligned} \qquad (14)$$

where
$e'^2 = e^2/(1 - e^2)$
$C_1 = e'^2 \cos^2 \phi^1$
$T_1 = \tan^2 \phi_1$
$N_1 = a/(1 - e^2 \sin^2 \phi_1)^{1/2}$
$R_1 = a(1 - e^2)/(1 - e^2 \sin^2 \phi_1)^{3/2}$
$D = x/(N_1 k)$

N_1 is the radius of curvature of the ellipsoid perpendicular to a meridian, and R_1 is the radius of curvature along a meridian.

The longitude from the central meridian is, to first order, the angle subtended by the easting distance (x):

$$\lambda - \lambda_o = \frac{x}{kN_1 \cos\phi_1} = \frac{D}{\cos\phi_1} \tag{15}$$

Correction terms are third order and above in D:

$$\lambda = \lambda_o + [D - (1 + 2T_1 + C_1)D^3/6 + (5 - 2C_1 + 28T_1 - 3C_1^2 + 8e'^2 + 24T_1^2)D^5/120]/\cos\phi_1 \tag{16}$$

These transformations were coded and tested using a numerical example from Snyder (1987). In the example below, the latitude to be transformed is 40.5° and the longitude is 73.5°. Numerical values were examined to determine the necessity of higher degree correction terms in order to obtain accuracy on the order of one meter, since the series expansions above provide fractional meter accuracy.

For the forward transformation, the UTM distances are the arc lengths subtended by the latitude and longitude angles. Since the central meridian of UTM zone 18 is 75°, the longitude subtended angle is 1.5°. Some of the relevant values follow.

Radius of curvature along longitude at 40.5 deg (N)	6,387,330.5
Initial easting = scale x radius x angle subtended	127,104.1
Third degree in latitude correction	2.304
Fifth degree in latitude correction	-0.00128
Final calculated easting distance	127,106.4
Correct easting distance	127,106.5

Distance along central meridian to latitude 40.5 (M)	4,484,838.0
Initial northing = scale x M	4,483,044.0
Second degree in latitude correction	1,080.98
Fourth degree in latitude correction	0.154
Final calculated northing distance	4,484,124.7
Correct northing distance	4,484,124.4

The corrections do not add to the total exactly due to computer roundoff.

For the inverse transformation, the latitude and longitude angles are subtended by the UTM arc lengths.

Initial latitude based on spherical Earth	40.2972
Latitude using ellipsoidal radius	40.3656
Latitude at central meridian (ϕ_1) (called footpoint latitude)	40.5097
Radius of curvature along longitude at latitude ϕ_1 (N_1)	6,387,334.0
Radius of curvature along latitude at latitude ϕ_1 (R_1)	6,362,271.4
Second degree in easting correction	0.0097
Final calculated latitude	40.500
Initial longitude difference at latitude ϕ_1	1.5002
Third degree in easting correction	0.0002
Final calculated longitude distance	1.5000

FIS DATASET

The data sent to FIS were remapped into a UTM projection covering the FIFE study area. The region covered by these data is presented in Table 6. The image size is 512 x 512, with a pixel spacing of 30 m. Units for IR channels are brightness temperature (K) x 100 and the visible channels are in Wm^{-2} μm^{-1} $ster^{-1}$ X 100. The latitude/longitude files are in degrees x 100. The flight legs, times, and channels available are shown in Table 7. The MAMS FIS dataset is available by contacting:

Dr. D. E. Strebel
NASA/Goddard Space Flight Center
Code 923
Greenbelt, MD 20771

Data Quality

The dataset created for FIS is of very good quality. However, as with most datasets there are a few problems. The data in band 8 for all of the daytime passes has a "grainy" appearance due to a stuck bit which induced erroneous eight count variations in the raw data. Thus, the radiance values derived from this data reflect this variability. On the second daytime and the fourth nighttime passes there are regions of missing data in the northeast corner. In these regions the brightness temperature values were set to 0. Due to reflected solar radiation in the 3.7 μm band (channel 10) a few values exceed 328 K. Since the data have been scaled by 100 and the maximum value which can be stored in a 2-byte integer form is 32767, data values that exceed 327.67 K have been set to 32767. Finally, the raw data in channel 10 contained some "speckling" of bad raw values, which is manifested in the derived brightness temperatures. The cause of this problem is unknown.

Table 6. FIS Data coverage region

Corner	Earth Coordinates		UTM Coordinates	
	Latitude	Longitude	Northing	Easting
Northwest	39:07:05	96:36:48	4,332,380	706,350
Northeast	39:06:51	96:26:10	4,332,380	721,680
Southeast	38:58:34	96:26:28	4,332,380	721,680
Southwest	38:58:48	96:37:04	4,317,050	706,350

Table 7. MAMS FIS Data for each pass

Flight Leg	Day	Time		Channels
		LDT	UTC	
1	4 June 1987	11:01:49 11:04:29	16:01:49 16:04:29	2-8, 10-12[a]
2	4 June 1987	11:22:54 11:25:33	16:22:54 16:25:33	2-8, 10-12[a]
3	4 June 1987	11:43:32 11:46:12	16:43:32 16:46:12	2-8, 10-12[a]
4	5/6 June 1987	22:35:09 22:37:49	03:35:09 03:37:49	10-12[a]
5	5/6 June 1987	22:47:46 22:50:26	03:47:46 03:50:26	10-12[a]
6	5/6 June 1987	22:58:52 23:01:31	03:58:52 04:01:31	10-12[a]
7	5/6 June 1987	23:10:34 23:13:13	04:10:34 04:13:13	10-12[a]
8	5/6 June 1987	23:27:33 23:30:13	04:27:33 04:30:13	10-12[a]

[a]Although channel 9 is more sensitive than its redundant channel 10, spurious noise in channel 9 limited its usefulness.

JOURNAL OF GEOPHYSICAL RESEARCH (JGR) DATASET

MAMS data collected during the two flight days described above were used to support an investigation of the thermal variability of surface features over the FIFE region. This research is described in the JGR special issue on FIFE (November 1992). The data used are very similar to that submitted to the FIS and described in this report. Several differences exist between the data sets:

(1) only two day-time passes and two night-time passes were used,
(2) the data were navigated and co-registered based on only those times and not all times as in the FIS data set, and
(3) the data were remapped into a rectilinear coordinate system with 50-m resolution.

The data used in the FIFE JGR paper covered a 19 x 21 km area which was slightly larger than but centered on the FIFE study site and virtually identical to the domain of the FIS data set. For both the day and night flights only the first and last passes over the region were used (see Table 7 for times).

For the JGR dataset, MAMS data and derived products were remapped into a rectilinear coordinate system corresponding to the data region (FIFE study site). The resulting images contained 420 lines and 380 elements of data. For both days, the first of the two images in the time sequence was navigated and Earth located to within several pixels of ground control points described above. The second image was then registered to the first image using the procedures described in this report. This provided preliminary image co-registration. A 50-meter spacing between image points was produced by the remapping procedure using the overlapping pixel information. This provided finer detail in the derived products compared with undersampling the raw data to produce 100-m resolution.

Residual shifts in the navigation were measured at pixel spacings of 20 and fed into the remapping program to be used as a bias in the computation of the image coordinates. The resulting images from this procedure were co-registered to within one pixel over most of the study region for both day and night data.

SUMMARY

Airborne multispectral imagery from the Multispectral Atmospheric Mapping Sensor (MAMS) were collected over the First ISLSCP Field Experiment (FIFE) on two days during Intensive Field Campaign - 1 (IFC-1) to study the time and space variability of remotely-sensed geophysical parameters. MAMS data were collected for three daytime passes on June 4 and five nighttime passes on June 5, 1987 over the site. The high spatial resolution of the sensor and low single sample noise in the visible and infrared channels allowed for an indepth analysis of the spatial variability of several derived geophysical parameters (Jedlovec and Atkinson, 1992). The radiance data and derived products were remapped and rectified to common coordinates so that multi-scene analysis of the data was possible. The multi-temporal nature of the data set provided valuable insight to the use of time change parameters from remote sensing platforms.

REFERENCES

Greenhood, D., 1964: *Mapping*. University of Chicago Press, 289 pp.

Hillger, D. W., and T. H. Vonder Haar, 1988: Estimating noise levels of remotely sensed measurements from satellites using spatial structure analysis. *J. Atmos. Ocean. Tech.*, **5**, 206-214.

Jedlovec, G. J., 1987: Determination of atmospheric moisture structure from high resolution MAMS radiance data. Ph.D. Thesis, The University of Wisconsin-Madison, 173 pp. [available University Microfilms International, 300 North Zeeb Road, Ann Arbor, MI 48106-1346].

_____, 1990: Precipitable water estimation from high resolution split window radiance measurements. *J. Appl. Meteor.*, **29**, 863-877.

_____, and R. J. Atkinson, 1992: Variability of geophysical parameters from aircraft radiance measurements for FIFE. *J. Geophys. Res.*, **97**, 18,913-18,924.

_____, K. B. Batson, R. J. Atkinson, C. C. Moeller, W. P. Menzel, and M. W. James, 1989: Improved Capabilities of the Multispectral Atmospheric Mapping Sensor (MAMS). NASA TM-100352, 80 pp. [available NTIS N89-20430].

_____, W. P. Menzel, R. Atkinson, G. S. Wilson, and J. Arveson, 1986a: The Multispectral Atmospheric Mapping Sensor (MAMS): Instrument Description, Calibration, and Data Quality. NASA TM-86565, 37 pp. [available NTIS].

_____, W. P. Menzel, G. S. Wilson, and R. J. Atkinson, 1986b: Detection of mountain induced mesoscale wave structures with high resolution moisture imagery. *Second Conference on Satellite Meteorology/Remote Sensing and Applications*, AMS, Williamsburg, VA, pp. 365-369.

Menzel, W. P., G. J. Jedlovec, and G. S. Wilson, 1986: Verification of small scale features in VAS imagery using high resolution MAMS imagery. *Second Conference on Satellite Meteorology/Remote Sensing and Applications*, AMS, Williamsburg, VA, pp. 108-111.

Moeller, C. C., L. E. Gumley, K. I. Strabala, and W. P. Menzel, 1989: High resolution depiction of SST and SSC from MAMS data. *Fourth Conf. on Satellite Meteorology and Oceanography*, AMS, San Diego, CA, pp. 208-212.

_____, W. P. Menzel, and K. I. Strabala, 1990: High resolution atmospheric and surface variability from combined MAMS and VAS radiances. *OSA Topical Meeting on Optical Remote Sensing of the Atmosphere*, Optical Society of America, Reno, Nevada.

Pearson, F., 1990: *Map projections: Theory and applications*. CRC Press, 372 pp.

Sellers, P. J., and F. G. Hall, 1987: First ISLSCP Field Experiment (FIFE): Experiment Plan, 177 pp. [available from NASA/Goddard Space Flight Center, Code 923, Greenbelt, MD 20771].

Sellers, P. J., F. G. Hall, G. Asrar, D. E. Strebel, and R. E. Murphy, 1988: The First ISLSCP Field Experiment (FIFE). *Bull. Amer. Meteor. Soc.*, **69**, 22-27.

Snyder, John P., 1987: *Map projections--A working manual*. U. S. Geological Survey Professional Paper 1395, 383 pp.

Wilson, G. S., 1984: Automated mesoscale wind fields derived from GOES satellite imagery. *Conf. Satellite Remote Sensing and Applications*, AMS, Clearwater Beach, FL, pp. 164-171.

APPENDIX

Raw data values (in units of radiance) are shown for each pass in Figure A1. The aircraft flight tracks are plotted as straight lines after correction using the landmarks. UTC times are indicated at each directional arrow. The images are rotated so that the flight tracks are in the proper direction with respect to the Earth. The FIFE study region is outlined. The distortions in this square region are due to differing pixel overlaps in the along track and scan directions, and the increase in ground coverage with scan angle, which compresses the image noticeably at large scan angles. The missing data values at the edges of the last two passes are due to aircraft roll.



Figure A1. MAMS raw imagery with the flight track information and the FIFE study region (outlined) for each of the passes shown in Table 7.

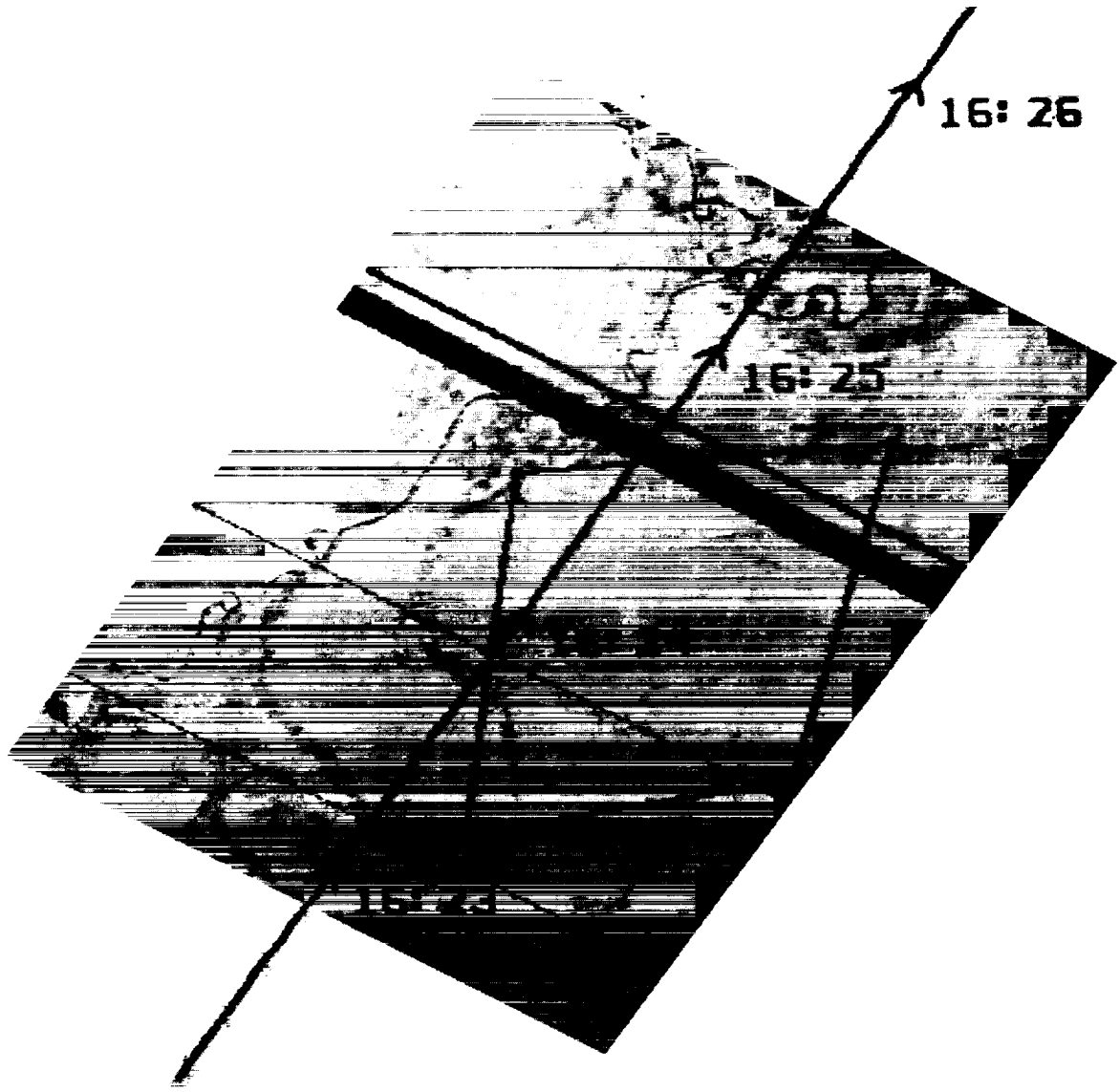


Figure A1. (continued)

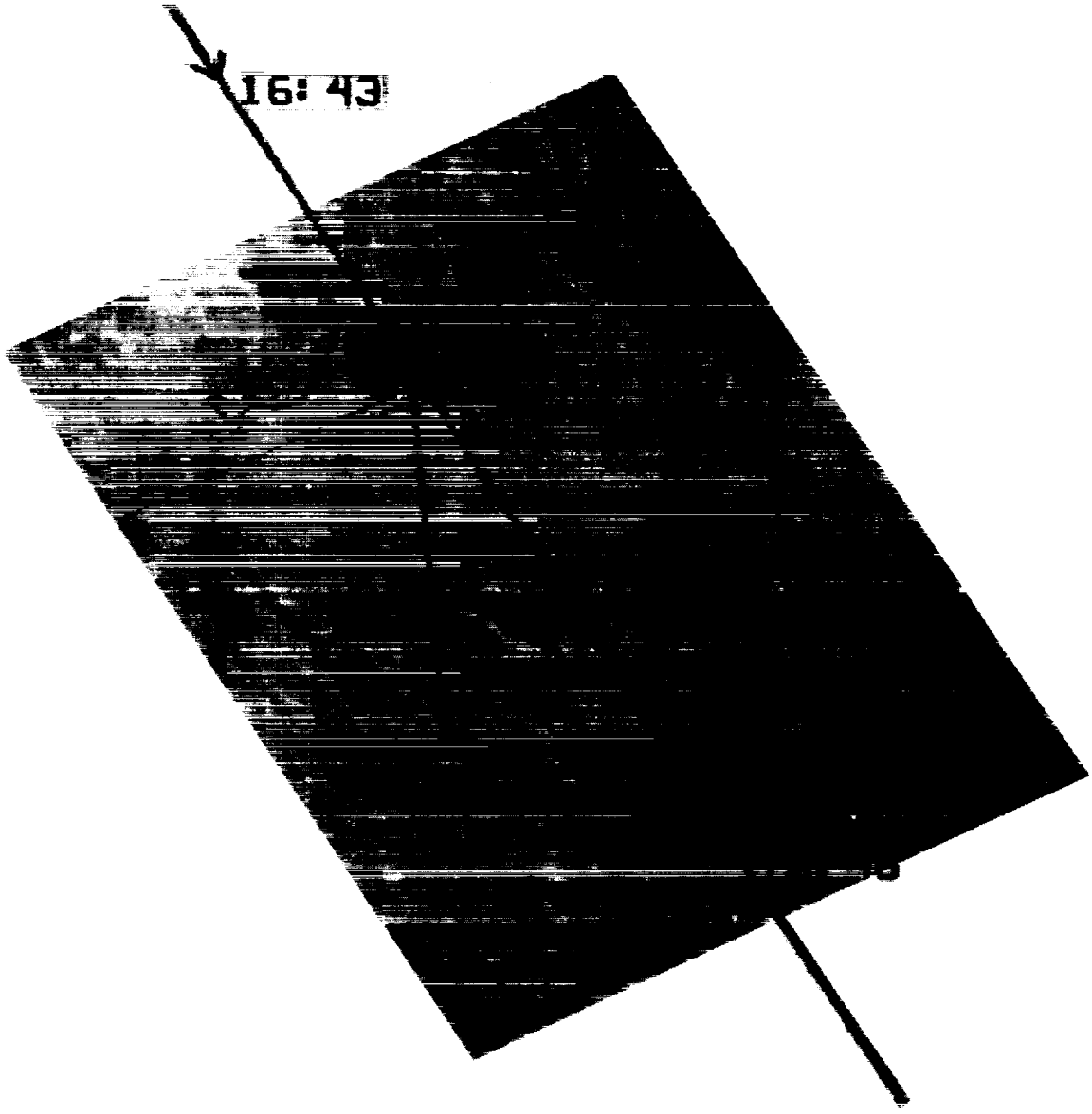


Figure A1. (continued)

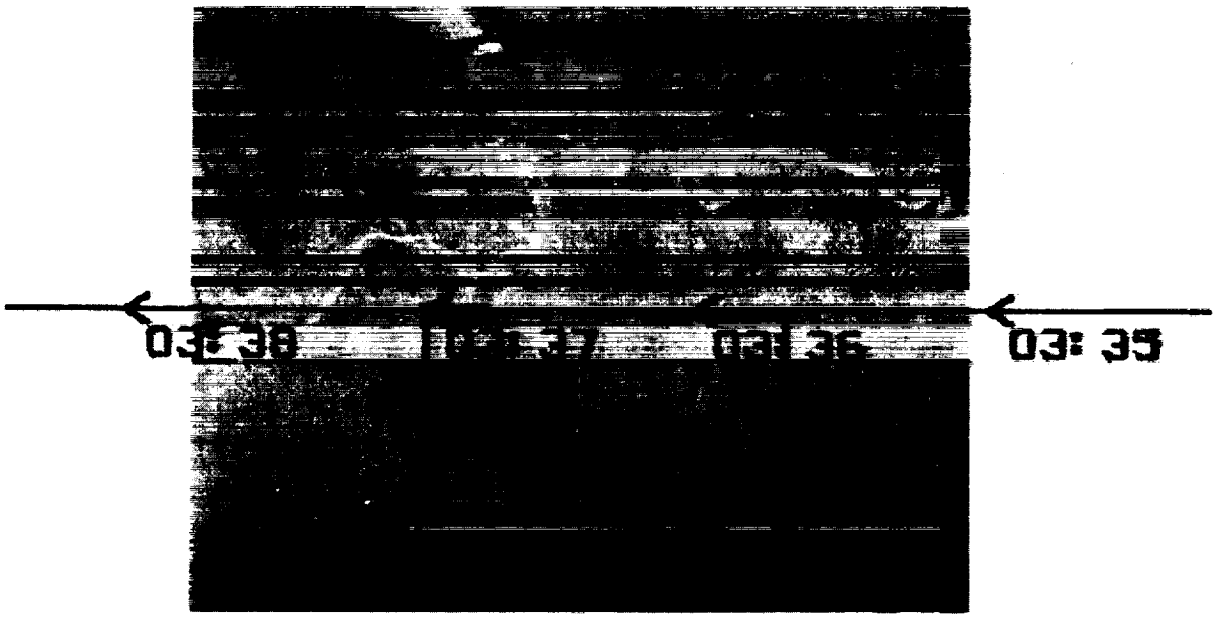


Figure A1. (continued)

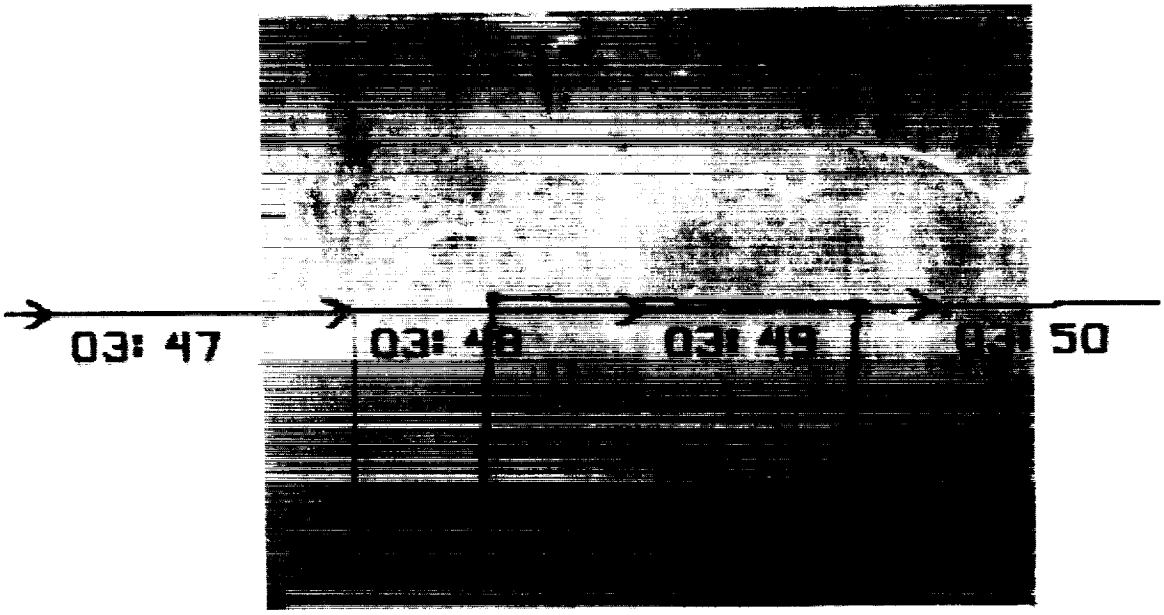


Figure A1. (continued)

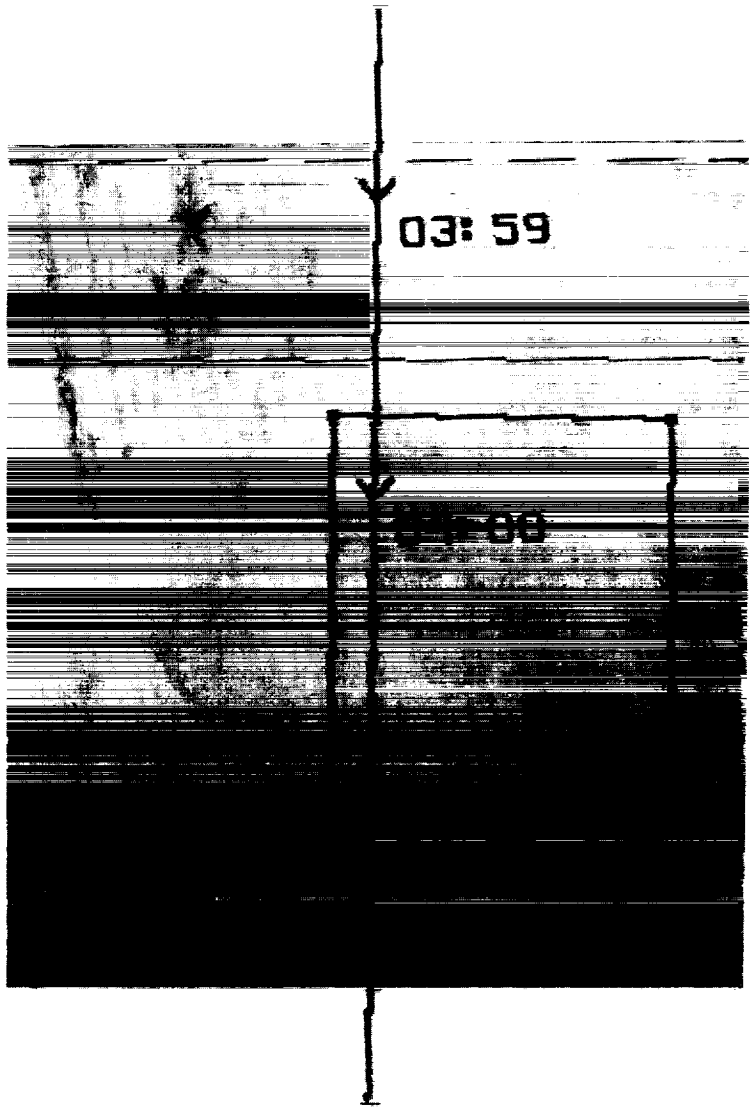


Figure A1. (continued)

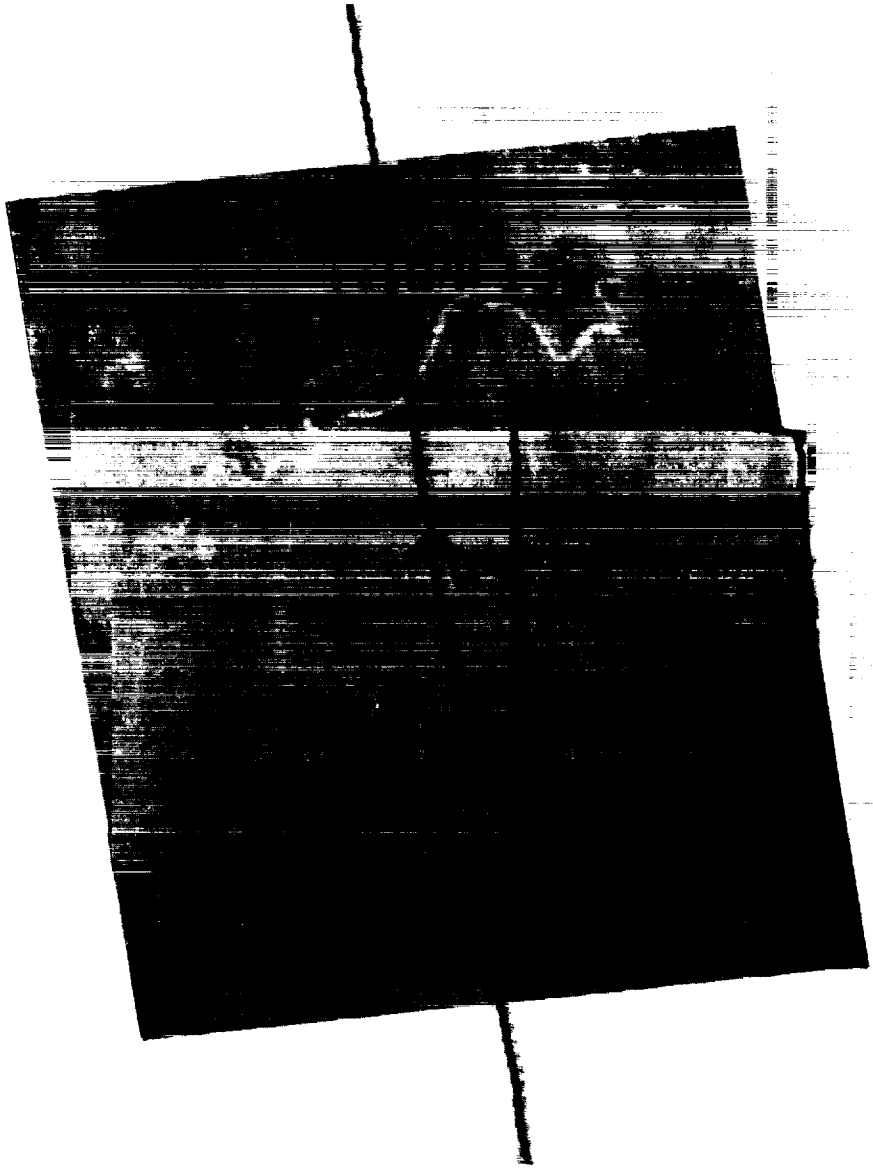


Figure A1. (continued)

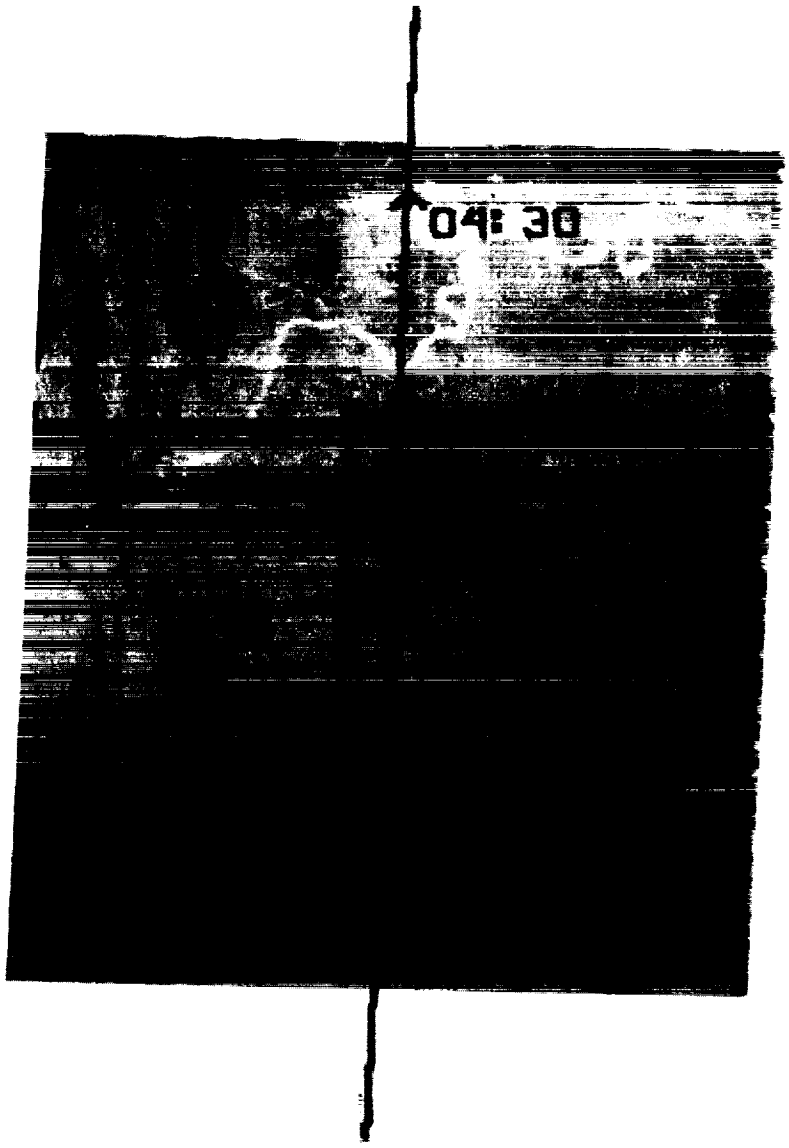


Figure A1. (continued)

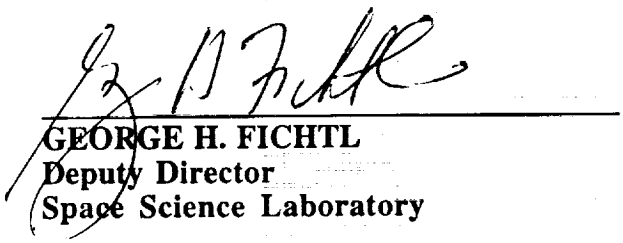
APPROVAL

CALIBRATION, NAVIGATION, AND REGISTRATION OF MAMS DATA FOR FIFE

By

G. J. Jedlovec and R. J. Atkinson

The information in this report has been reviewed for technical content. Review of any information concerning Department of Defense or nuclear energy activities or programs has been made the MSFC Security Classification Officer. This report, in its entirety, has been determined to be unclassified.



GEORGE H. FICHTL
Deputy Director
Space Science Laboratory

☆ U. S. GOVERNMENT PRINTING OFFICE 1993 733–050 / 80039